Development of a new methodology to analyse the fluid flow within an internal combustion engine using one and three - dimensional numerical technology

By

Rory Sinclair

A thesis submitted to the Faculty of Engineering, Department of Mechanical Engineering of the University of Glasgow for the degree of Doctor of Philosophy (PhD.)

March 2003

Conducted at Volkswagen AG, Wolfsburg, Germany

Acknowledgements

I thank everyone who helped me to the complete this work. I am grateful especially to Dr. Timothy Strauss and Dr. Peter Schindler from Volkswagen and Prof. Brian Scott from the University of Glasgow for their support and advice.

This work could not have been done except with the support of my family.

ABSTRACT

Computational predictions allied to fast prototyping methods speed design in the fiercely competitive automotive industry. Volkswagen A. G. models unsteady, external-flows around and within its vehicles by the methods of computational fluid dynamics (CFD). Solutions of models constructed on circa 10 million fluid elements consume upwards of 1200 CPU hours.

Transient flows in inlet and exhaust manifolds determine the capacity of internal combustion engines to breathe. Power, flexibility, economy and emissions are at risk. Space constraints and the complexities of turbo-charging, emission control devices etc. exercise engine designers. Perforce, they resort to compact and essentially three-dimensional form manifolds. Computationally efficient one-dimensional approaches are defeated. Furthermore, the experimentally determined loss coefficients upon which they depend are inaccessible.

This research would reduce the size and complexity of CFD models and speed their computation by analysing engine manifolds into regions where one-dimensional methods suffice to capture the flow and contiguous regions where strong, three-dimensional influences prevail. New methods discovered secure the boundaries between one and three-dimensional regions, having regard to the conservation laws and differing numerical representations of the communicating flows. This hybrid computational scheme and an associated design methodology are tested and demonstrated herein. The hybrid methodology is broadly applicable to flows of compressible and viscous fluids in multi-connected ducts.

STAR-CD, a commercial code developed by Computational Dynamics Limited, is the chosen three-dimensional modeller. This system comprises STAR (Simulation of Turbulent flow in Arbitrary Regions), a solver that employs an implicit, finite-volume method, and PROSTAR, a user interface which combines pre and post processors. Volkswagen's engine development department has used STAR-CD successfully and in diverse applications since the early 1990's.

PROMO, the chosen one-dimensional code, is a joint development by the Institute of Engineering Design and the Computer Centre of the Ruhr-University of Bochum. The solver employs an explicit, finite-difference method that is intrinsically efficient: a single-processor, SGI Octane workstation can calculate the flow in a complete internal combustion engine in under two hours. Ingineurbuero Linnhof continues to develop PROMO, which is an integral element of Volkswagen's engine development process.

Semi-automatic meshing of the internal volume of a subject manifold by SAMM, an Adapco software product, generated predominately hexahedral meshes. However, layers of "prism cells" constructed near walls lent accuracy to calculations in the boundary layer. Transient flow fields being unpredictable *ab initio,* an elegant resolution of the flow relied upon adaptations of the 3-D mesh. Mesh quality control and validation applied ERCOFTAC

principles. A model constructed on 400,000 mesh elements served the pay-off between accuracy and cost.

Boundaries declared between three-dimensional and one-dimensional regions in hybrid models place differing flow interpretations and disparate computational schemes in juxtaposition. Unless made transparent, these boundaries must reflect spurious waves; artefacts created when pressure waves fall upon them. Transparency depends upon the correctness and coherence of data describing the physical flow and conformance of numerical representations of them.

Design criteria established herein prevent the imposition of boundary planes that translate a three-dimensional flow to one-dimensional form in regions containing reverse flows or at sites where markedly skewed velocity profiles persist. In the converse case, realistic boundary conditions must be established entering three-dimensional regions by inference from quasi, two-dimensional velocity profiles which interpret one-dimensional data prudently. A profile factor introduced that weights boundary data, consistently with the evolving three-dimensional field, defends, and preserves the conservation laws and principles.

Computational schemes that seek to make implicit and explicit solutions synchronous by causing one-dimensional and three-dimensional regions to overlap at boundaries prove prejudicial to the accuracy of the physical field. A boundary face method proposed avoids this difficulty at the expense of leaving the one and two-dimensional fields synchronous but phase shifted, one with respect to the other, by one time interval.

Though the prediction of flows throughout an entire engine is the aim, this exemplar – the proof of concept – examined flows in the inlet manifold of an Audi V6 TDI production engine. Audi experimental data, recording flows within the inlet manifold and their influences on engine performance, was sufficient to validate computed predictions.

The hybrid model predicted the measured volumetric efficiency characteristic accurately, though with the peak efficiency shifted towards higher speeds. Pressure waves generated by the operation of inlet valves mapped the experimental results correctly, with small departures in peak amplitude evident at high speeds. Phase changes evident in computed waveforms, consequent on increasing speed, reproduced the experimental evidence. The computational result predicted the known imbalance between the flows in the cylinder banks correctly.

The signal result for the hybrid methodology is its capacity to explain the engine characteristic through knowledge of flows occurring in the connecting pipe, i.e. to interpret and expand costly experimental observation that relied upon pressure transducers.

The hybrid methodology demonstrated its utility: it reduced the reliance on experimentation significantly; it predicted flows in complex manifolds economically; its accuracy was sufficient to drive performance enhancing engine developments. It stands secured within Volkswagen's declared engine process chain.

CONTENTS

LIST OF FIGURES

NOMENCLATURE

A	Area
ρ	Density
$\sqrt{g}$	Determinant of metric tensor
h	Enthalpy
p	Pressure
s_i	Momentum source components
s_h	Energy source
s_m	Mass source
t	Time
q	Heat flux
k_R	Friction losses
T	Temperature
τ_{ij}	Stress tensor
u_i	Absolute field velocity
u_j	Relative velocity between fluid and local (moving) coordinate frame
w	Velocity component (1D equations)
x_j	Cartesian co-ordinate (i = 1,2,3)
κ	Isentropic exponent
I_{vo}	Inlet valve open
I_{vc}	Inlet valve close
m_a	Mass of air induced into the cylinder per cycle
p_e	Environmental pressure
T_e	Environmental temperature
V_c	Swept volume

PUBLICATIONS

R. Sinclair; T. Strauss; P. Schindler: "Code Coupling, a new approach to enhance CFD analysis of engines"; SAE Technical paper 2000-01-0660. Paper presented at the SAE World congress in Detroit, Michigan, March 2000.

R. Sinclair; T. Strauss; P. Schindler: "Validated 1D/3D coupling method to solve transient flows in internal combustion engines"; ASME Technical paper. Paper presented at the ASME Congress in Vancouver, British Columbia, August 2002.

1 INTRODUCTION

Compliance with legislative constraints regarding atmospheric pollution, noise emissions and consumption of hydrocarbon fuels, requires engineers to create new design methodologies that are capable of still greater finesse than hitherto. Knowledge of the fluid flow within an internal combustion engine is increasingly relevant and critical. Successful development of the multiple physical elements and functions that constitute an internal combustion engine requires that the associated physical phenomena be predicted with greater certainty and at a sustainable cost. Predictions employing analytical methods and computational solutions are to the fore because of the high cost of hardware and experimental determinations and particularly so when the aim is to achieve a systematic optimisation of an entire engine. Analysis discloses the weak points of the product quickly and guides the introduction of systematic improvements. Measurements alone are never sufficient to determine the complex physical phenomena that occur in internal combustion engines. The focus here is on the optimisation of the charging phase and, therefore, on unsteady flow in a severally connected inlet manifold made compact by space restrictions.

Due to the complexity of engine processes, a complete multi-dimensional, time-dependent numerical calculation of an internal combustion engine is out of reach of current technology. Physical modelling of turbulence [1] is a critical issue affecting numerical calculations of flows explicitly; high Reynolds numbers occurring in complex engine geometries exacerbate this challenge. Large Eddy Simulation (LES) has advanced considerable in recent years. However, LES solves only the largest eddies; modelling the effect of the smallest ones remains dependent upon filtering the exact Navier-Stokes equations. The computational cost of LES, which in its nature is able to capture unsteadiness in flows, usually restricts the method to rather low Reynolds numbers, far from those typical of flows in practical engines [2]. In current automotive industry practice, the prediction of unsteady external flows depends upon models constructed on circa 10 million fluid elements. A solution may require upwards of 1200 CPU hours using a cluster of 32 processors [3]. Engine flows are inherently complicated in nature because there exists more than one dynamically changing variable. The behaviour of the intake and exhaust systems is especially complex. Transient flows in them interact and regulate the air that that the engine breathes, the fuel burned and, consequently, the power it produces. The determination of complex flows in manifolds constitutes a major challenge to engine designers.

The power of Computational Fluid Dynamics (CFD) to predict complex fluid flows has grown significantly; the increasing power of computational platforms makes its application more practical and economic. The automobile industry has adapted CFD to its peculiar needs innovatively. The modelling of engine processes continues to develop as the industries basic understanding of the physics and chemistry within engine components expands. Numerical modelling can make major contributions to engineering developments at different levels of

generality or detail. According to Heywood [16], the several stages of model development lead to a more complete understanding of the process under study, provide guidelines for more rational (thus less costly) experimental efforts, and predict engine behaviour over a wide range of design and operating variables.

Calculations of one-dimensional (1D) unsteady flows have employed techniques such as the method of characteristics [4, 5] and finite difference approaches [17] in an extended period. These 1D methods rely, variously, on several assumptions. For example, the flow over the entire cross-section of a pipe is represented by data prescribed at a single node or point in 1D analyses. A one-dimensional model that will yield acceptable results may not be constructed except with the benefit of experimentally determined data [6]. This is especially so when 3D flow effects dominate in determining loss mechanisms. Thus, a 1D model will depend for its propagation by a numerical scheme on experimentally determined loss coefficients. Blair, G. P. *et al* [50] discover the risks that attend the deduction of discharge coefficients from measured data and discuss the inaccuracies that result from their incorporation in engine simulations.

Increased computational power has brought the modelling of three-dimensional domains into prospect. The mid-Eighties saw the expansion to multidimensional modelling techniques, so called due to their inherent ability to provide detailed information of the flow field based on the solution of the governing flow equations [7]. However, the development of computational power was not then mature and was insufficient to cope with the increasing aspirations of the application engineer. By the early nineties, it was possible, for practical purposes, to calculate steady flows within intake manifolds [8, 9].

The production of a suitable numerical mesh for large engine components still requires vast engineering skill and considerable time (measured in numbers of weeks), the power of current mesh generation techniques [10] notwithstanding. Three-dimensional numerical modelling of the entire flow within a complete engine remains inaccessible; set-up time and computational costs are prohibitive. The prospect examined here is that the application of 3D CFD methods be restricted to regions in the physical system where three-dimensional flows prevail and generate losses not easily captured experimentally. One-dimensional representations shall suffice elsewhere. The computational description of the engine components is simplified; mesh generation and computation are speeded; engine design is facilitated.

However, the application of valid flow states at the several boundaries formed between the 1D and 3D regions of a hybrid model constitutes a significant problem.

Unsteady conditions exacerbate the boundary definition problem: How are unsteady boundary conditions determined? How do 1D and 3D computations interact at boundaries between these disparate numerical schemes? Boundary conditions may be prescribed using the results of exploratory 1D numerical solutions [11]. However, the imposition of fixed boundary conditions prevents feedback between the 3D modelled component and systems external to it. New methods developed herein overcome major elements of this generic problem that now impedes the simulation of fluid flows in entire engine systems and, therefore, engine designers.

The motivation for this thesis was to develop a new methodology to predict the local and global gas motion within internal combustion engines accurately. Therefore, this work aims to obtain a complex, time dependant solution for a multi-dimensional modelled component and to find a solution for the entire engine system. Current, state-of-art CFD techniques are to be adapted to this new method.

The research was undertaken at the Volkswagen engine development department in Wolfsburg, Germany in association with the department's fluids group. Therefore, the conclusions posed in this report are primarily of interest to industrial applications. However, the outcome sought was a numerically stable fluid dynamics method that sustains the conservation laws and was validated by experimental data..

Chapter 2 presents the underpinning theories of the one- and three-dimensional numerical techniques, upon which the hybrid is constructed. The flow equations that are solved are represented mathematically. Turbulence modelling required for 3D modelling is described. Finally, the evolution of numerical techniques required is detailed. An explicit approach adopted in the 1D case permits fast computation for each time step, subject to a condition placed on the step size. The 3D technique adopts an implicit approach, which is free from this stability constraint but demands a significantly greater computational power.

Chapter 3 presents the new methodology. It starts with a review of boundary conditions and differentiates between parabolic and elliptical boundary condition used in this work. Information exchange is a central topic: the methods used to transfer flow data between the 1D and 3D techniques are described in detail. Care is taken to ensure conservation of fluid within the system and that the conservation laws are upheld more generally. The mechanism whereby a quasi three-dimensional flow distribution may be inferred from a one-dimensional result at the entry to a three-dimensional region is described. The limitations of this technique are juxtaposed with the higher fidelity of the representation obtained in the three-dimensional region.

Boundary face and the overlap methods of discretisation introduced are compared. The modelling procedures necessary to sustain the new methodology are introduced. In this context, the initialisation of the flow domain is an important issue. Methods that will restart a hybrid calculation that is interrupted and sustain the computation without loss of time are described. A further point of importance discussed in this chapter is the consideration of turbulence quantities affecting boundaries of the 3D model

Chapter 4 provides an evaluative case. Properties of the coupling interface are examined by its application to a simple test geometry. A comparison with a 1D calculation of the test geometry provides an initial validation of the new methodology. The possibility that reflections might be generated at interfaces of 1D and 3D regions is a concern. This validation examines the efficacy of the mechanism that infers a quasi three-dimensional boundary condition at entry to a three-dimensional region of the hybrid.

Chapter 5 applies the hybrid methodology to the inlet manifold of a six-cylinder, turbocharged direct-injection diesel engine, an Audi product. The charge air pipe strongly affects the engine's volumetric efficiency, depending upon the engine speed. Computational

and experimental data are compared at engine speeds of 2000, 3000 and 4000 rpm. The sensitivity of the computed prediction to the placement of the interface between the 1D and 3D systems is examined. A detailed description of the predicted 3D flow field proffered exemplifies the effect of engine speed on the flow in the charge pipe. The unsteady nature of the flow in the charge air pipe is evident. An alternate pipe geometry posed to improve the volumetric efficiency proved inauspicious; the efficiency fell. None the less, the purpose of developing the new methodology was achieved and demonstrated: the modified geometry was quickly and efficiently constructed and analysed, without the need for experimentally determined data.

The research has provided a powerful operational tool that relies on no more than best-practice commercial CFD codes. A generic scheme demonstrated enables the analysis of complex internal flow geometries into contiguous one-dimensional and three-dimensional regions, with signal reductions in computational time and costs won.

2 FLUID MECHANICS AND NUMERICAL SOLUTIONS

2.1 One-Dimensional Flows

2.1.1 Background

Most engine simulation programs employ one-dimensional analyses of the flow. The pay-off is between computational speed and accuracy; the dependence is on experimentally determined loss coefficients [17]. The presumption of one dimensionality neglects variations in fluid properties and of the velocity transversely to the direction of flow. Thereby, the analysis of transient flows of compressible fluids is simplified and considerably speeded. Experimental correlations of loss coefficients permit the estimation of losses in straight pipes with good accuracy. More problematic are discontinuities at pipe junctions and steps in the cross-sectional area and e.g. in orifices, combustion cylinders and plenum. Control volumes placed at these discontinuities must rely upon experimentally estimated loss coefficients. For the purposes of 1D analysis, the properties pressure and temperature and the fluid velocity and local speed of sound (p, T, w a) suffice to describe the process of gas exchange within an engine.

2.1.2 Mathematical Representation

The following hyperbolic partial differential equations describe one-dimensional, irreversible flow of a compressible medium:

$$\frac{\partial \rho}{\partial t} + \frac{\partial}{\partial x}(\rho \cdot w) = -w \cdot \rho \frac{d \ln A}{dx} \qquad \textit{Eq. 2.1}$$

$$\frac{\partial}{\partial t}(\rho w) + \frac{\partial}{\partial x}(\rho w^2 + p) = -\rho w^2 \frac{d \ln A}{dx} - k_R \cdot \rho \qquad \textit{Eq. 2.2}$$

$$\frac{\partial}{\partial t}\left(\rho \frac{w^2}{2} + \frac{P}{\kappa - 1}\right) + \frac{\partial}{\partial x} w\left(\rho \frac{w^2}{2} + \frac{\kappa}{\kappa - 1} p\right) = -w\left(\rho \frac{w^2}{2} + \frac{\kappa}{\kappa - 1} p\right) \frac{d \ln A}{dx} + q \qquad \textit{Eq. 2.3}$$

In the above: ρ represents the thermodynamic property density, k_R is the friction force on mass element $\rho \cdot A \cdot dx$, A is the cross-sectional area of the pipe (which may be a function of the grid spacing), q is the rate of heat transfer from external sources and x and t are position and time co-ordinates respectively [20]. Equation *2.1* ensures mass conservation; equation *2.2* preserves momentum; equation (*2.3*) conserves energy.

Stromberg [21] makes the friction factor k_R available from the following:

$$F_R = k_R \rho A d_x \qquad \textit{Eq. 2.4}$$

And,

$$F_R = \frac{\lambda}{d} \rho \frac{w^2}{2} \frac{w}{|w|} A d_x . \qquad \textit{Eq. 2.5}$$

The quotient $w/|w|$ in the latter allows the friction force to act in opposition to the flow. The coefficient λ is a constant, commonly set to 0.019 [22]. The mean pipe diameter is d.

2.1.3 Numerical Method

This set of partial differential equations (PDE's) is transformed into a set of simultaneous algebraic equations, referenced to a sequence of grid points in the flow domain, so that it may be solved numerically. PROMO, the one-dimensional gas dynamics code adopted, uses a finite difference method to effect this transformation and solve the algebraic equations. This method employs computational power conservatively.

2.1.3.1 Discretisation

Figure 2.1 below illustrates the discretisation of a 1D model of a pipe on a set of axial nodes. A solution of the flow is calculated at each internal grid point. Marked black, the boundary nodes denote either the environmental boundaries of the system or the location of control volumes representing multi-dimensional discontinuities in the flow.

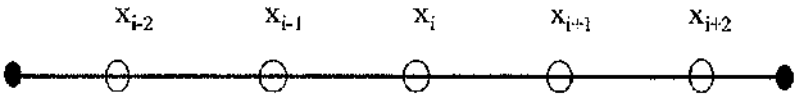

● Boundary node

○ Internal node

Figure 2-1: Example of a 1D grid

The differential equations are approximated by difference equations at each grid point that refer to the values at surrounding nodes. The values of the variables at the node and at a number of neighbouring nodes are related in a single algebraic equation generated at the node. The first and second derivatives of the variables with respect to the co-ordinates may be approximated by a series expansion according to Taylor's theory, or by polynomial fitting of the data. The accuracy of the solution increases as the spacing of the grid points reduces. However, this improvement is won at the cost of a rising computational duty, as the number of equations increases [23]. The maximum distance permitted between computational grid points is limited by the CFL stability criterion.

The methodology adopted here utilises the two-step Lax – Wendroff [17] technique to solve the flow equations. This method employs a second order central differencing scheme with respect to the spatial co-ordinate. For this purpose the pipe equations are written in vector form:

$$\frac{\partial G}{\partial t} = -\frac{\partial F}{\partial x} - C \qquad \textit{Eq. 2.6}$$

With G equal to the variable vector

$$G = \begin{bmatrix} \rho \\ \rho w \\ \rho \dfrac{w^2}{2} + \dfrac{p}{\kappa + 1} \end{bmatrix} \qquad \textit{Eq. 2.7}$$

The transformation of the differential equation into an equation of differences is accomplished by the Taylor approximation of the function $G(x,t)$ at point $P(x,t)$ of the t,x plane.

Using central differencing to express the spatial derivative leads to:

$$G_{i+1/2}^{n+1/2} = \frac{1}{2}\left(G_{i+1}^{n} + G_{i}^{n}\right) - \frac{\Delta t}{2\Delta x}\left(F_{i+1}^{n} + F_{i}^{n}\right) - \frac{\Delta t}{4}\left(C_{i+1}^{n} + C_{i}^{n}\right) \qquad \textit{Eq. 2.8}$$

and finally,

$$G_{i}^{n+1} = G_{i}^{n} - \frac{\Delta t}{\Delta x}\left(F_{i+1/2}^{n+1/2} + F_{i-1/2}^{n+1/2}\right) - \frac{\Delta t}{2}\left(C_{i+1/2}^{n+1/2} + C_{i-1/2}^{n+1/2}\right). \qquad \textit{Eq. 2.9}$$

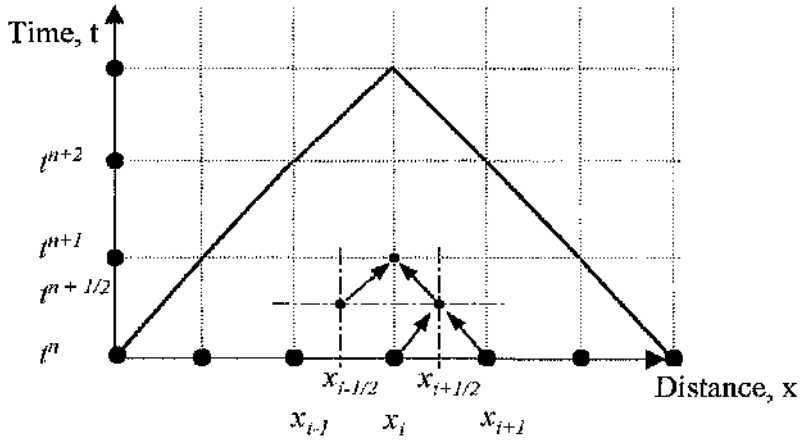

Figure 2-2: Schematic of two step Lax-Wendroff numerical method

The two-step Lax-Wendroff technique is illustrated above. Flow information at a new time t^{n+1} is calculated in terms of data derived from the previous time step. It is a two-step method: the first step proceeds from t^n to an intermediate time $t^{n-1/2}$, the second step propagates the solution to t^{n+1}. Flow information at the grid points x_i and x_{i+1} is used to solve

up to the intermediate time $t^{n+1/2}$, and yield results for a grid point $x_{i+1/2}$. This procedure is carried out for the neighbouring grid points, namely x_{i-1} and x_i, thereby calculating flow information for grid point $x_{i-1/2}$ for time $t^{n+1/2}$. The second step uses these two newly found grid points to find flow information at time t^n for grid point x_n.

The Lax-Wendroff technique finds an explicit solution of the problem, i.e. values at the new time step are found explicitly from values resulting from the previous time step.

The explicit approach generates difference equation containing only one unknown, which can be solved explicitly for this unknown. The finite-difference module contained within the dashed line shown below illustrates this scheme

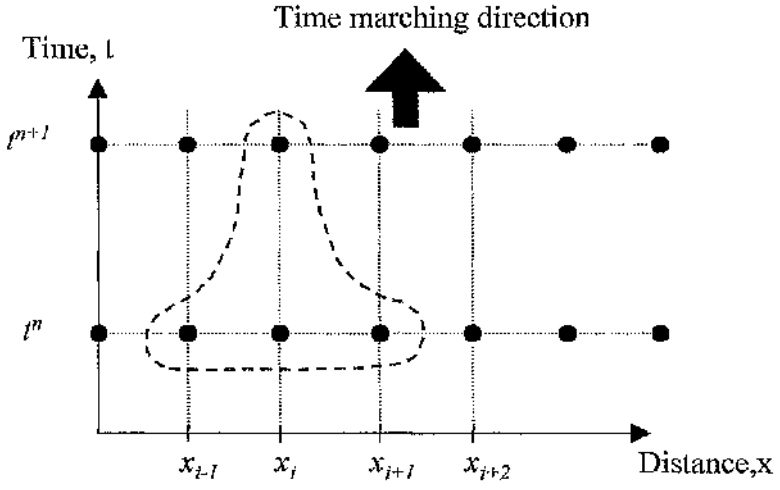

Figure 2-3: Finite difference temporal displacement

The Courant-Friedrichs-Lewy (CFL) condition determines the stability required for the explicit approach adopted by the above finite difference method. A description of this criterion is given here because of its importance to later discussions. The CFL criterion is defined with the following equation [25]:

$$C = w\frac{\Delta t}{\Delta x} \qquad \textit{Eq. 2.10}$$

This criterion is the ratio of the advection of a fluid particle in a chosen time interval to the spatial resolution of the computational grid and must not exceed unity, illustrated graphically in the following figure.

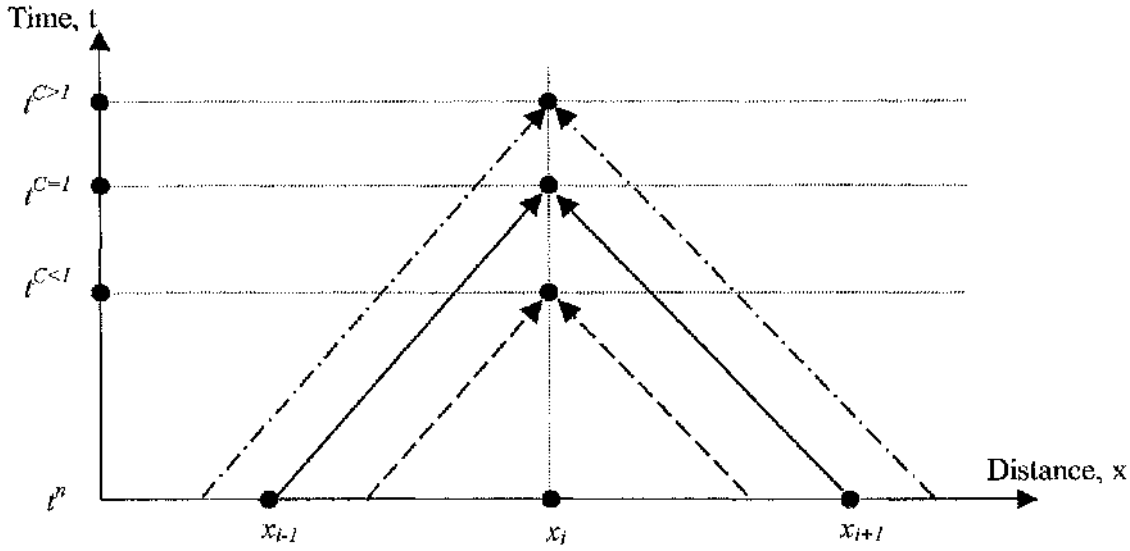

Figure 2-4: Time step size restrictions when CFL number is utilised

Values at a new time step are found explicitly from flow information derived in the previous time interval. Assuming a CFL number of unity, the new time step information $t^{C=1}$ is found from flow information at x_{i-1}, x_i and x_{i+1}.

The slope in x, t describes the transport of acoustic waves propagating in the flow, right and left of the centre node x_i. The area within the triangle, triangle (x_{i-1}, t^n), (x_{i+1}, t^n) and $(x_i, t^{C=1})$, is defined as the analytical domain [49]. Flow conditions are then defined inside this analytical domain. For times that correspond to a CFL number less than unity, the new value x_i at time $t^{C<1}$ can be calculated, since the new point lies within the analytical domain. Evidently, the converse is true for time intervals that correspond to CFL numbers greater than unity. This criterion notwithstanding, errors may occur in the inversion of the matrix of the coefficients of the algebraic equations when the latter is poorly posed.

2.1.3.2 Boundary Conditions

To render the solution unique [26], conditions at the domain boundaries (Dirichlet-type boundary condition) must be prescribed. Additionally, the 1D method requires that losses at the intersections between pipes and at discontinuity (orifice, volume, etc.) are represented by appropriate coefficients. The several conditions that apply to these discontinuities are described in detail in [21, 23].

2.2 Three-Dimensional Flow

2.2.1 Background

STAR-CD (**S**imulation of **T**urbulence in **A**rbitrary **R**egions, by **C**omputational **D**ynamics, London), a commercially available 3D CFD code [27, 28], is employed.

This code solves the Navier – Stokes equations describing unsteady flow of incompressible or compressible fluids and accommodates several turbulence models. An implicit, higher order difference scheme was employed to discretise the time dependent flow equations.

STAR-CD is a versatile code. Automotive companies use it to predict external flow fields around large-scale models, e.g. the aerodynamics of car shape, and to study the detail of unsteady combustion process, e.g. in the vicinity of pistons moving within the cylinder block [15].

Parallel processing is permitted to accommodate very large models. Thus, different processors may simultaneously compute the flow in several contiguous regions of a large model.

2.2.2 Mathematical Representation

The following provides a brief overview of the three-dimensional equations describing the unsteady flow. Reference [27] provides an exhaustive discussion. Turbulence modelling is discussed, sufficient to justify the choice made.

2.2.2.1 General Equations

The mass and momentum conservation equations for incompressible and compressible fluids (the Navier Stokes equations) in Cartesian tensor notation are:

$$\frac{1}{\sqrt{g}}\frac{\partial}{\partial t}(\sqrt{g}\rho)+\frac{\partial}{\partial x_j}(\rho\tilde{u}_j)=s_m \qquad \textit{Eq. 2.11}$$

$$\frac{1}{\sqrt{g}}\frac{\partial}{\partial t}(\sqrt{g}\rho u_i)+\frac{\partial}{\partial x_j}(\rho\tilde{u}_j u_i-\tau_{ij})=-\frac{\partial p}{\partial x_i}+s_i \qquad \textit{Eq. 2.12}$$

Correspondingly, the energy equation is,

$$\frac{1}{\sqrt{g}}\frac{\partial}{\partial t}(\sqrt{g}\rho h)+\frac{\partial}{\partial x_j}(\rho\tilde{u}_j h-F_{h,j})=\frac{1}{\sqrt{g}}\frac{\partial}{\partial t}(\sqrt{g}p)+\tilde{u}_j\frac{\partial p}{\partial x_j}+\tau_{ij}\frac{\partial u_i}{\partial x_j}+s_h \qquad \textit{Eq. 2.13}$$

In the foregoing, h is the static enthalpy, defined by:

$$h\equiv\bar{c}_pT-c_p^0T_0+\sum m_mH_m=h_t+\sum m_mH_m \qquad \textit{Eq. 2.14}$$

In these results repeated subscripts denote summation, for example,

$$\frac{\partial}{\partial x_j}(\rho u_j)=\frac{\partial(\rho u_1)}{\partial x_1}+\frac{\partial(\rho u_2)}{\partial x_2}+\frac{\partial(\rho u_3)}{\partial x_3} \qquad \textit{Eq. 2.15}$$

2.2.2.2 Turbulence Modelling

Turbulence modelling techniques adopted herein are discussed in [13, 14, 18].

When the flow exceeds a critical Reynolds number, turbulence generated within the body of the flow dissipates momentum. The scale of the turbulence is small compared to the computational grid size at Reynolds numbers encountered in engine manifolds. Numerical modelling of turbulence is necessary if the associated losses are to be estimated.

Two-equation turbulence models are available to model the diffusion, when the length scale is not required as an empirical input. Variants of the well-known k - ε model, comprising transport equations for the turbulent energy k and its dissipation rate ε, are adapted to general applications such as pipe flows. The options differ from each other in one of the following respects:

- The form of the equations
- The treatment of the near-wall region
- The constitutive relations that relate Reynolds stresses to the rates of strain.

The standard k - ε model used is discussed here briefly. The wall functions employed are introduced.

The k - ε turbulence model calculates the turbulent energy and the energy dissipation via two separate equations. These equations for k and ε are made elliptic by the gradient formed of the diffusion term. Their solution depends upon the application of suitable boundary conditions [29].

The standard model uses the following transport equations:

$$\frac{\partial(\rho k)}{\partial t} + div(\rho k U) = div\left[\frac{\mu_t}{\sigma_k} grad k\right] + 2\mu_t E_{ij} \cdot E_{ij} - \rho\varepsilon \qquad \textit{Eq. 2.16}$$

$$\frac{\partial(\rho \varepsilon)}{\partial t} + div(\rho \varepsilon U) = div\left[\frac{\mu_t}{\sigma_\varepsilon} grad \varepsilon\right] + C_{1\varepsilon}\frac{\varepsilon}{k} 2\mu_t E_{ij} \cdot E_{ij} - C_{2\varepsilon}\rho\frac{\varepsilon^2}{k} \qquad \textit{Eq. 2.17}$$

They contain five adjustable constants C_μ, σ_k, σ_ε, $C_{1\varepsilon}$ and C_2. Data fitting across a comprehensive range of turbulent flows [30] generates constants suitable for general applications, *vide* the table below.

C_μ	σ_k	σ_ε	$C_{1\varepsilon}$	C_2
0.09	1.00	1.22	1.44	1.92

2.2.2.3 The Wall Region

Near-wall calculations rely on the so-called "law of the wall". This method patches a prescribed semi-empirical function to a basic model. The wall function specifies how turbulence varies near the wall and is sensitive to pressure gradients, which make the function 'non-equilibrium'. Assumptions of quasi-equilibrium fail when the flow is separated, impinging or highly skewed. Predictions depend on the patching point and are sensitive to the near-wall meshing.

If a Reynolds number based on a distance y from the wall is formed, the value y is in the order of the length scale in the flow direction. Inertia forces dominate far from the wall. As y decreases to zero the Reynolds number based on y also decrease to zero. For y small, a region exists where Re_y is on the order of unity. At this distance from the wall and closer to it, the viscous forces equal or exceed inertia forces. Thus, in flows contained within solid boundaries a substantial region of inertia-dominated flow exists far away from the wall, whilst a thin layer, dominated by viscosity and not greatly influenced by the external flow, stands adjacent to the wall. Therefore, the mean flow velocity depends principally on the distance y from the wall, the fluid density ρ, the viscosity μ and the wall stress τ_w. Dimensional analysis yields:

$$u^+ = \frac{U}{u_t} = f\left(\frac{\rho u_t y}{\mu}\right) = f(y^+) \qquad \textit{Eq. 2.18}$$

This is the law of the wall. Note that the appropriate velocity scale is $u_t = (\tau_w/\rho)^{1/2}$, being the so-called friction velocity.

The wall function representation of the boundary layer is accurate depending on the degree to which the assumptions correspond to the reality of the application. In the 3D code used in this work, the main assumptions on which the wall functions [13] are based are

- Variations of velocity etc. are predominantly normal to the wall.
- Effects of pressure gradients and body forces are negligibly small.
- Shear stress and velocity vectors are aligned and unidirectional throughout the layer.

- Energy production and dissipation are balanced.
- The variation of the turbulent length scale is linear.

The resulting formulae giving the cross-stream profiles in terms of the normal distance y from the wall are [18]

$$u^+ = \begin{cases} y^+ & , y^+ \le y_m^+ \\ \frac{1}{\kappa}\ln\left(Ey^+\right) & , y^+ > y_m^+ \end{cases}$$

2.2.3 Numerical Method

2.2.3.1 Approach

The schematic of Fig. 2-5 depicts the numerical approach adopted in the 3D methodology.

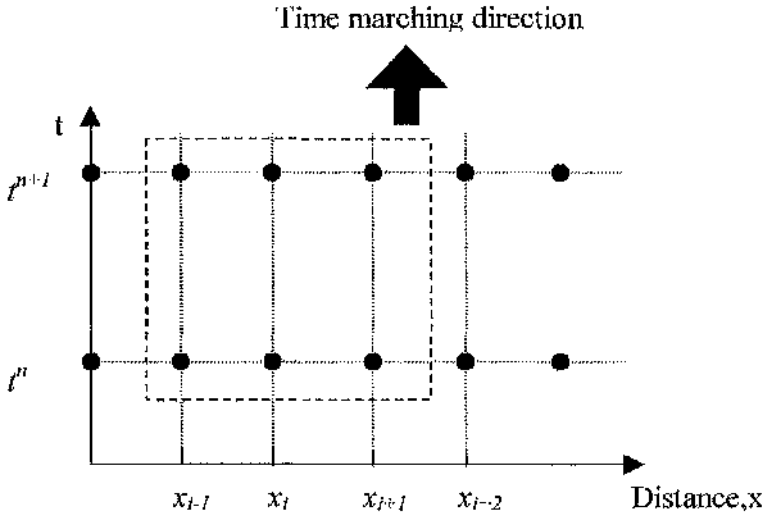

Figure 2-5: Time development using the implicit approach

Filled circles represent a computational node in the 3D flow domain. Flow information for node x_i at a new time level t^{n+1} is calculated from neighbouring, nodes x_{i-1} and x_{i+1}, at time level t^n and at time level t^{n+1}. Therefore, a system of algebraic equations must be written for each interior grid point and solved simultaneously all the unknowns. This is the basis for an implicit solution. By definition, an implicit approach is one where the unknowns must be obtained by means of a simultaneous solution of the difference equations applied to all the grid points arrayed at a given time level.

The implicit approach is more complex than is the explicit approach, and especially so when the demands on memory are compared.

In the explicit approach, the choice of Δx and the application of the CFL stability criterion determine Δt. The implicit approach [49] is not so subject to stability restrictions. Indeed, stability can be maintained for much larger time steps than would be admissible in an explicit solution. Furthermore, some implicit approaches are unconditionally stable [26], i.e. stable solutions are available independently of Δt. An implicit approach can span a given time interval with considerably fewer steps than is required by an explicit scheme. Therefore, though the implicit approach, being relative complex, demands more computational time per time, shorter run times result in faster computation overall.

In practice, the fully implicit formulation imposes limits on the time step size. Numerical errors increase at large time steps. Therefore, it is important to have a time step that is small enough to limit the temporal approximation errors to acceptable values.

2.2.3.2 Discretisation

The 3D code employs the finite volume method [16, 17]. This section describes the sub-dividing technique adopted for the spatial dimensions.

The solution domain is sub-divided into a finite number of small control volumes (CVs) by a grid that defines the boundaries of the volumes. An example of a typical CV described in a Cartesian grid is shown in Fig. 2-6

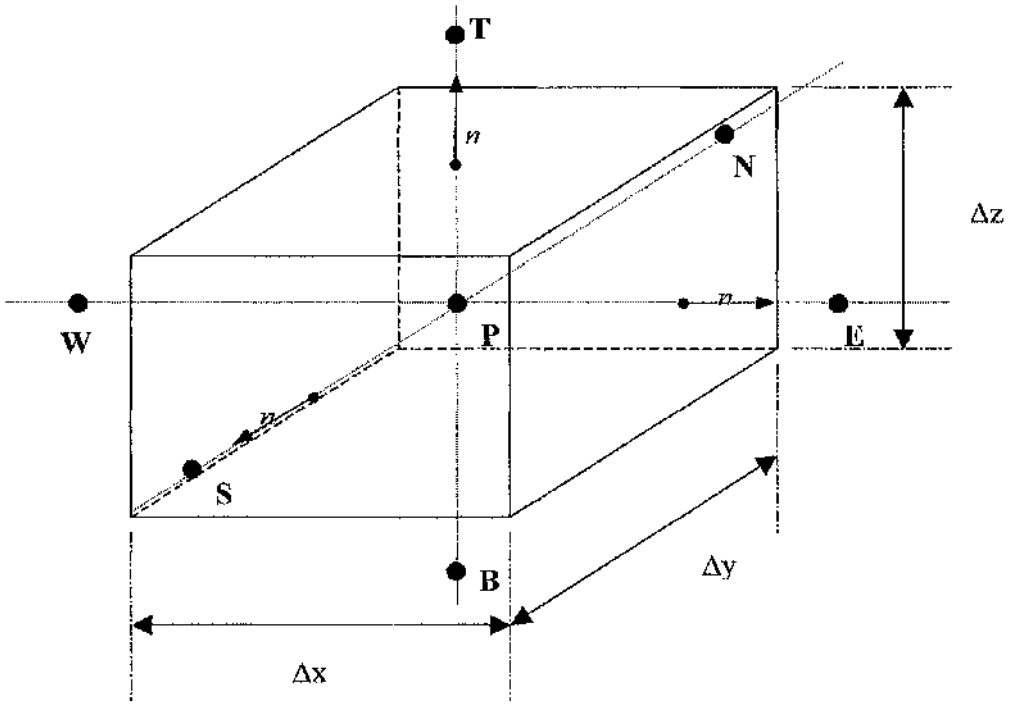

Figure 2-6: Control volume for the finite volume discretisation method

The finite volume method starts with the integral form of the conservation equations, viz:

$$\int_S \rho\phi v \cdot ndS = \int_S \Gamma grad\phi \cdot ndS + \int_\Omega q_\phi d\Omega \qquad \textit{Equ. 2-19}$$

S denotes an integral taken over the surface of the CV; Ω denotes a volume integral. To obtain an algebraic equation for each CV, the surface and volume integrals must be approximated by quadrate formulae.

The CV surface can be sub-divided into six plane faces (for a 3D hexahedral cell flow domain). Maintenance of conservation requires that the CVs shall not overlap; each cell face is unique to the two CVs that lie on either side of it. The simplest approximation is provided by the midpoint rule: the integral is the product of the integrand at the cell face centre and the cell face area. Since the values at the cell face centre are not known *a priori* they have to be

obtained by interpolation. A number of interpolation practices are available [18, 13]. A higher order scheme was adopted.

2.2.3.3 Differencing Scheme

In order to march the calculation forward in space (i.e. from one node to the next) an appropriate interpolation scheme is required. A second-order differencing scheme was adopted for the purposes of coupling calculations. This scheme operated in two steps

- Using a multidimensional Total Variation Diminishing (TVD, [39]) scheme, a set of monotone gradients was computed for the cell-face flow properties.
- These cell-face properties are used to compute the face fluxes for all advected properties using a monotone and bounded advective scheme.

This scheme allows an accurate, second-order spatial discretisation. The advective scheme controls the accuracy with which sharp discontinuities may be captured (i.e. shock waves in compressible flow fields).

A high accuracy on distorted meshes is proved by this method and at the same time is bounded, ensuring that physically non-negative quantities are always positive. This method was used for velocities and turbulence quantities, but is less useful for enthalpy, since it is non-linear. The code developers recommended this method. Furthermore, Shaw et al. [14] observed good comparisons with experimental tests with this differencing scheme.

2.2.3.4 Boundary Conditions

All CFD problems are defined in terms of initial and boundary conditions. The initial values must be specified for all of the flow variables at all solution points (grid points) in the flow domain. It is extremely important that well posed, realistic boundary conditions are applied; otherwise, severe difficulties will be encountered in obtaining solutions.

Depending on the type of boundary used, the code requires boundary values of pressure, temperature, velocity and turbulence quantities. A two-dimensional cell layer is placed at each geometrical boundary; each layer can then be individually defined so that appropriate flow boundaries are placed along with wall type boundary conditions. The boundary conditions are constant over the entire time step. Thereby, a quasi-steady analysis of the fluid flow in the 3D domain is impressed for the duration of each time step.

3 THE HYBRID MODEL

This chapter discusses interfacing schemes that underpin the new methodology. A detailed description of the primary features of the interface methodology is proffered and illustrated. Required understanding for this work is the definition of boundary conditions. Turbulence modelling requires special attention. Concluding comments concern the code programming

3.1 Physical Interfaces in Hybrid Models

3.1.1 Introduction

Before a flow system can be analysed numerically, fluid conditions must be specified at the system boundaries. Two general categories of boundary conditions arise: wall boundaries representing geometrical restrictions (i.e. pipe walls) and boundaries through which fluid may enter or leave elements of the system (i.e. regions where a defined mass flow, pressure, etc. are prescribed). Flow properties must be specified over an entire boundary region, irrespective of the numerical methodology used. An accurate specification for each of these boundary types ensures a correctly posed problem.

While the flow inlet and exit boundaries of a 3D model are usually treated as 2D surface elements, flow conditions in a 1D methodology are, due to the nature of the 1D calculations, impressed onto a single boundary node.

3.1.2 Boundary Definition

Inlet and exit boundary regions of an exhaust system for one bank of a Volkswagen W8 spark ignition internal combustion engine are illustrated in Fig. 3-1. This modelling provides for analysis of the catalyst, pipe system, etc.

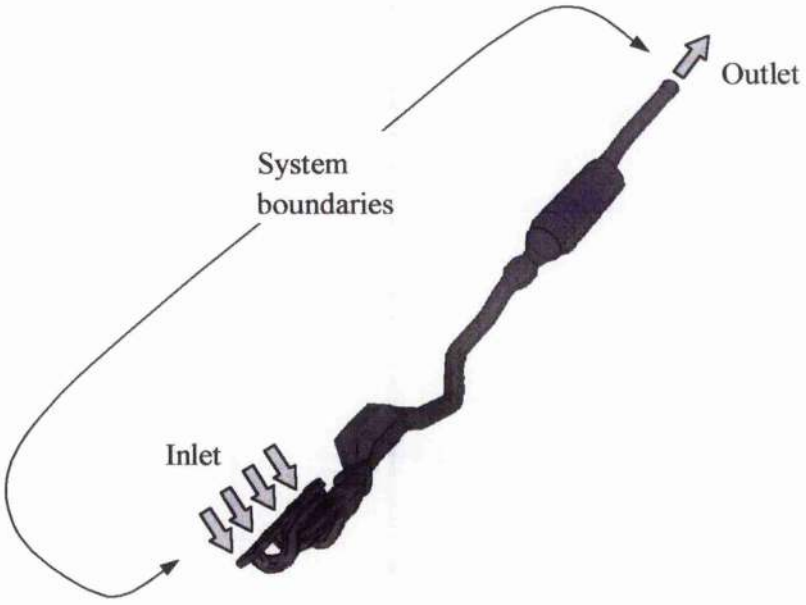

Figure 3-1: Boundary definition of an exhaust system

The behaviour of the flow inside the system is dependent on the geometry of the system and the boundary conditions. Physically the boundary conditions may be constant or vary in time.

Time dependent boundary conditions can be defined in two ways. A one-way flow situation is such that the conditions at a location are influenced by changes in flow conditions on one side of that location alone. A two-way situation is such that the conditions at a given location are influenced by changes in flow conditions on either side of that location.

Patankar [40] says that these computational concepts correspond to the mathematical terms parabolic and elliptic: one-way behaviour corresponds to the parabolic form; two-way behaviour corresponds to the elliptic form.

Characterising the flow situation at the boundary in this way allows the differentiation of time varying conditions. The parabolic definition prescribes conditions before the start of the calculation (commonly known as list or table input method). The elliptic definition specifies the boundary conditions throughout the duration of the calculation (method utilised in a 1D/3D hybrid model).

Fig. 3-2 illustrate these arguments.

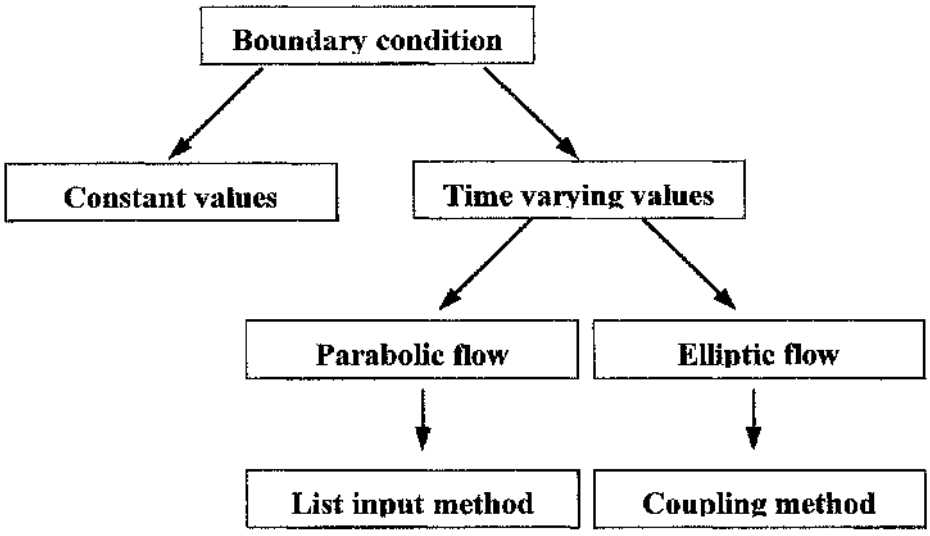

Figure 3-2: Differentiation of Boundary conditions

3.1.2.1 Constant Value Boundaries Conditions

Constant boundary conditions allow the analysis of flow in a steady state. This allows the validation of the calculated flow field with experimental results, e.g. Tippelman test bench for in-cylinder flow.

A main advantage of this type of boundary definition is that it is relatively easy to specify. Furthermore, since the flow field is to converge to a steady state, the time independent equations are used for the flow calculations thereby reducing computational time and memory resources. [Hard to understand where this leads, not that it does actual harm]

3.1.2.2 Time varying Boundary Conditions

- Parabolic

The most widely used method to apply time varying boundary conditions in industrial 3D CFD applications is to apply states determined in a 1D, stand-alone calculation of the system [11]. On completion of the 1D calculation, flow states at boundary sites of the 3D model are extracted at each time interval and listed. This method requires that the component of interest be solved twice: firstly as an element of the complete 1D model and secondly as an independent 3D model.

Experimental testing of the system may provide a part or all of this boundary information. Alternatively, pre-defined mathematical flow functions may be employed.

When boundary conditions taken from a complete 1D representation of the engine system – i.e. one that includes a 1D rendered version of a 3D element - are prescribed to a 3D

numerical mode in this manner, the 1D system model stands isolated the finer resolution of the complex component notwithstanding. Lack of feedback between the models prejudices the predictions.

- Elliptic flow

This method avoids the deficiency described above; it is employed in this work. The complex component that must be rendered in 3D is made integral with the extended engine system that contains it, the latter rendered in 1D. The hybrid model so created permits the complexity of the 3D modelled region to interact physically with 1D representation of systems external to it.

Figure 3-3 is a 1D schematic of a six-cylinder turbo-charged internal combustion engine. The arrows indicate flow directions within the system. The component modelled in 3D – the inlet manifold in this case – is contained in the box above cylinder bank 2, shown with dashed lines. The 3D and 1D models share differently expressed but physically and computationally consistent interpretations of boundary conditions set at the dashed boundaries. Herein lines the challenge that this method poses.

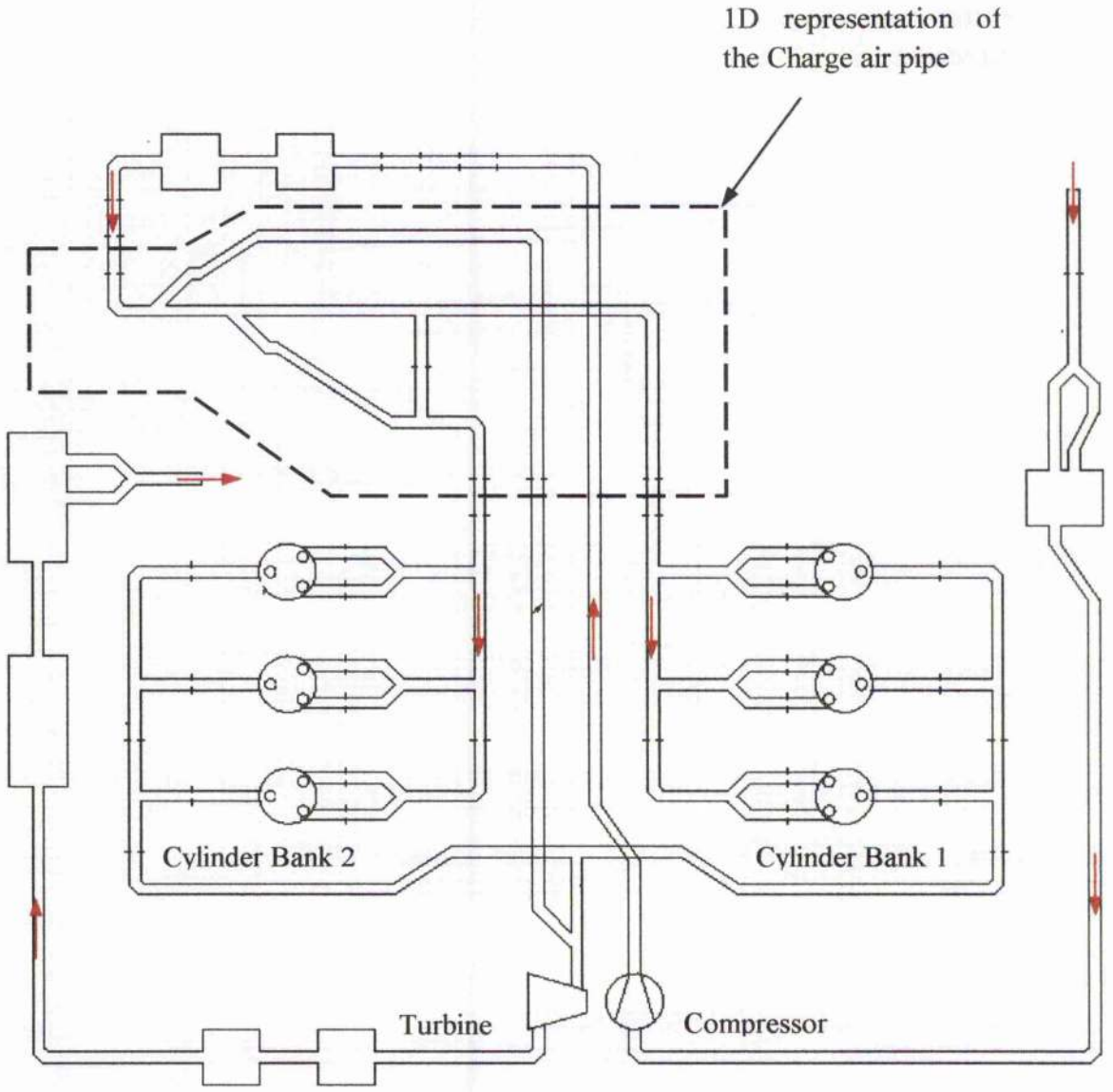

Figure 3-3: Schematic depicting model containing elliptic boundary conditions

3.1.3 Engineering the Interfaces

3.1.3.1 Physical Data Transferred from 3D to 1D Domains

Physical data that are subject to a conservation law must be summed over the entire cross-section of the boundaries that separate 3D and 1D models. The following equations sum non-uniform distributions in 3D flows.

The density of an ideal gas is expressed by:

$$\rho = \rho(p,T) \qquad \textit{Eq. 3.1}$$

Mass continuity requires that mass flows computed on either side of a boundary are equal:

$$\sum_{i}^{n} \dot{m}_{i,3D} = \dot{m}_{1D} \qquad \textit{Eq. 3.2}$$

Elaborating on this gives:

$$\left[\sum_{i}^{n}\left(\frac{p_i w_i A_i}{RT_i}\right)\right]_{3D} = \left[\frac{\overline{p}\cdot\overline{w}A}{R\overline{T}}\right]_{1D}. \qquad \textit{Eq. 3.3}$$

The following condition applies to the impulse function:

$$\sum_{i}^{n} M_{i,3D} = M_{1D}, \qquad \textit{Eq. 3.4}$$

At the interface:

$$\left[\sum_{i}^{n}\left(\dot{m}_i w_i + p_i A_i\right)\right]_{3D} = \left[\dot{m}_{1D}\overline{w} + \overline{p}A\right]_{1D}. \qquad \textit{Eq. 3.5}$$

Conservation of energy requires:

$$\sum_{i}^{n} H_{0i,3D} = H_{0,1D}, \qquad \textit{Eq. 3.6}$$

which condition is met when

$$\left[\sum_{i}^{n}\dot{m}_i\left(c_p T_i + \frac{1}{2}w_i^2\right)\right]_{3D} = \left[\dot{m}_{1D}\left(c_p\overline{T} + \frac{1}{2}\overline{w}^2\right)\right]_{1D}. \qquad \textit{Eq. 3.7}$$

For the entropy

$$\sum_{i}^{n} s_{3D} = s_{1D}, \qquad \textit{Eq. 3.8}$$

which is described as follows

$$\left[\frac{1}{\dot{m}_{total}}\sum_{i}^{n} s_i \dot{m}_i\right]_{3D} = s_{1D}. \qquad \textit{Eq. 3.9}$$

The subscript i refers to the cell number at the 3D boundary, which is summed over the total number of cells, n, for the boundary region. The codes require values of pressure, temperature and velocity at the interfaces.

The foregoing over-specifies the problem: there being three unknown quantities, three equations suffice. Traupel [41] showed that an accurate transfer from a non-uniform distribution to a single mean value could not be achieved, irrespective of the equation set adopted. He demonstrated that equations 3.3, 3.5 and 3.7 lead to an increase in the entropy. Following Traupel's assertion, though not propagating it, Appendix 8.2 demonstrates that the entropy increase is minimal. Furthermore, the entropy equation is not needed except to determine the direction in which the processes occur [48].

This study does not encompass e.g. disequilibria of species or of chemical reactions. In any case, the interfaces it establishes, if subject to representational and computational errors, are *ipso-facto,* reversible artefacts. In this work, the decay of the stagnation pressure represents energy dissipation, being the result of shear stresses. Loss coefficients in 1D flows and turbulence modelling in 3D domains estimate the dissipation. The equation of state determines the entropy, viz $s = s(p,T)$. The stagnation temperature is constant; the solution obtains p and v. Ergo, the solution finds the entropy. This work does not accommodate rate processes driven by disequilibria.

3.1.3.2 Physical Data Transferred from 1D 3D Domains

The task is to interpret information contained in a single 1D boundary node and construct a 2D boundary condition that is a sufficient representation of the flow entering the 3D domain. Industrial CFD applications set uniform distributions of the properties and the velocity over the boundary region. A coupling interface described here constructs a two-dimensional distribution – one that preserves the conservation laws – and, subject to design rules, applies it to the 3D boundary.

3.1.4 Transverse Velocity Profiles at interfaces

Industrial 3D CFD practice artificially extends the model geometry upstream of the inlet boundary region so that flow entering the boundary is developed. An artificial extension such as this is impractical when adjacent regions of a system must remain contiguous, as in the case of a hybrid construct.

For time varying flow calculation the standard procedure is to apply a block profile at the 3D boundary (a constant value impressed over the entire boundary region). A high Reynolds number CFD calculation that relies upon a "wall function" to evaluate the shear stress, so initiated, inevitably produces a flow distribution similar to that shown below (figure 3-6). Therefore, the application of a block profile onto the boundary region is inadmissible; the 3D flow field will be seriously awry.

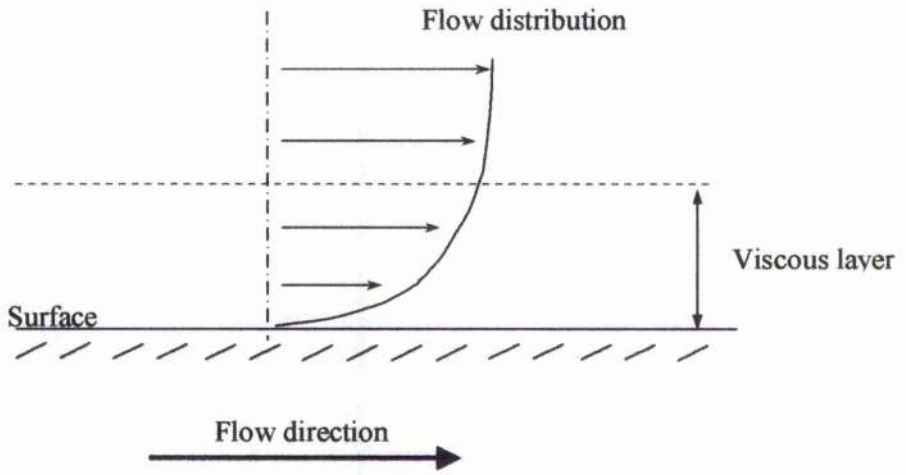

Figure 3-4: Near wall flow profile

3.1.4.1 Inference, Relying on Correlations of Experimental Results

According to this method, the flow distribution is inferred from correlations of experimental results, judged as representative of the upstream geometry [42]. Simple cases can be entertained, vide Figure 3-5 that represents axi-symmetric flow in circular pipes. However, a markedly skewed velocity distribution stands in a pipe preceded by a sharp bend, Figure 3-6. The paucity of data for non-circular cross section pipes is a major impediment to this method of inference.

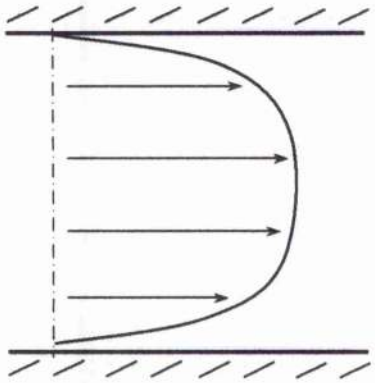

Figure 3-5: Symmetrical flow profile

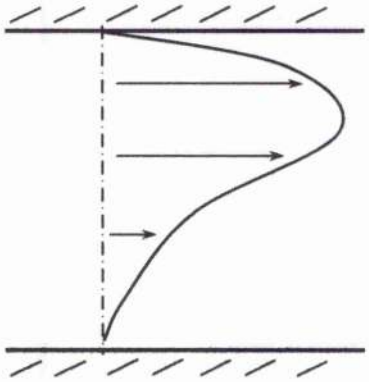

Figure 3-6: Asymmetrical flow profile

3.1.4.2 Application of Coupling Constraints

With the application of the hybrid model, time varying flow information is known on both sides of the interface. Individual cell information in the 3D model at the coupling interface

and the 1D flow information directly neighbouring the interface can be used to define a new flow distribution onto the boundary region of the 3D model, described in detail below.

The individual cell values and the summed value over the cross-section are used to find a profile factor, which is defined by:

$$factor = \frac{\phi_i}{\phi_{total}} \qquad \text{Eq. 3.10}$$

where ϕ represents the fluid conservation law to be considered (i.e. mass flow) and the subscript i denotes the cell number. The subscript total refers to the total value passing through the boundary region.

New and individual boundary cell conditions, weighted according to the profile factor, are derived from incident 1D data and applied at entry to the 3D flow domain.

This method ensures a flow distribution similar that previously calculated inside the 3D flow domain. Flow distributions such as those shown in Figures 3-7 and 3-8 are accommodated.

Another phenomenon, which may occur, is a change in flow direction at the boundary region from one time step to the other. When a reversal of flow occurs, time step restrictions will ensure that the velocity is small at the interface regions. The coefficients found above will flip the flow distribution at the boundary to coincide with the new flow direction received from the 1D model.

Shown below, (Fig. 3-7), is a distribution that contains a region of reversed flow.

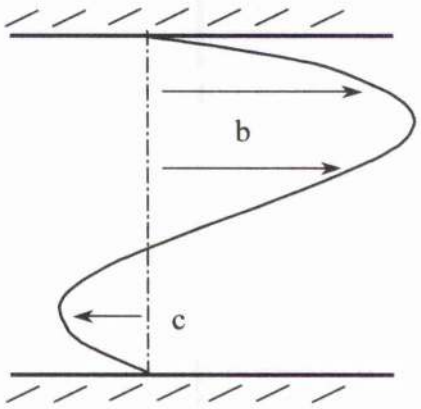

Figure 3-7: Illustration of reversal flow, where flow enters and leaves a domain

This boundary condition is not easily defined; the interface must be shifted to a more closely one-dimensional section in the pipe framework. Equations 3.3, 3.5 and 3.7 do not accommodate reversed flows.

The coupling strategy proved satisfactory: the program did not crash, but flagged a warning whenever it encountered an adverse velocity profile requiring an intervention.

Two assumptions implicit to the flow distribution approach are:

- Since flow distribution coefficients found at the end of one 3D time step are applied to the definition of new boundary conditions for the subsequent time step, the form of the flow distribution (for each conservation equation) is assumed not to change markedly during a single time step.
- The field inside the 3D region determines gradients of flow properties at coupling interfaces. The 1D information determines the magnitude of the properties and the velocity.

3.2 Discretisation at Interfaces

3.2.1 Coupling Strategy

Two strategies to couple 1D and 3D CFD codes were evaluated. The first exchanges information at the boundary faces of each model, two variants of the second cause the 1D and 3D models to overlap.

3.2.1.1 Boundary Face Coupling

Figure 3-8 demonstrates the principle of the coupling strategy.

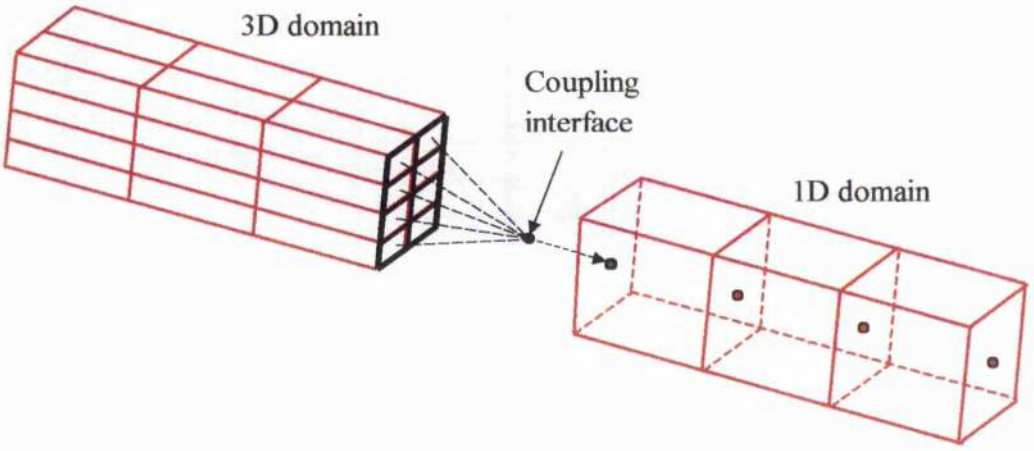

Figure 3-8: Boundary face coupling

The coupling interface is a plane separating the 1D and 3D flow boundaries. Information being calculated at the centre of the fluid cells, not at the boundary layer, the interface plane is informed by the cell layer neighbouring the 3D boundary region, which data is used in the averaging procedure.

Implicit is the assumption that fluid properties are constant throughout individual cells. Care taken during grid generation in the 3D region to create a thin cell layer adjacent to the 3D boundaries minimised the risk incurred.

Information is passed from the 1D model to the 3D model immediately it is instantiated in the 1D boundary node. Therefore, no extra conditions apply to the 1D grid near a 1D/3D interface.

3.2.1.2 Overlap Coupling

Overlap coupling creates a small region in which 1D and 2D solutions are generated coincidentally, but independently.

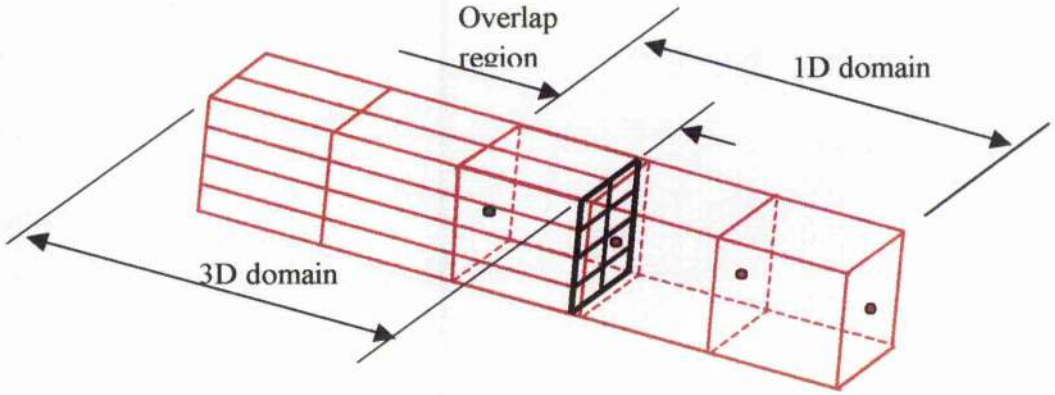

Figure 3-9: Schematic of the Overlap coupling method

The strategy utilises the Lax-Wendroff technique adopted in the 1D methodology (vide Chapter 2). Data at three neighbouring nodes calculated at the end of the preceding time interval are used to determine the state of the flow during the succeeding time interval.

3.2.1.3 Fluid properties from 1D domain to 3D domain

Allowing a region of overlap as shown in figure 3-9, the boundary information for the 3D flow domain is obtained from inside the 1D flow domain. When the overlap region is equal to the grid spacing adopted in the 1D calculation, the 3D boundary information is obtained from the last internal node before the 1D boundary node.

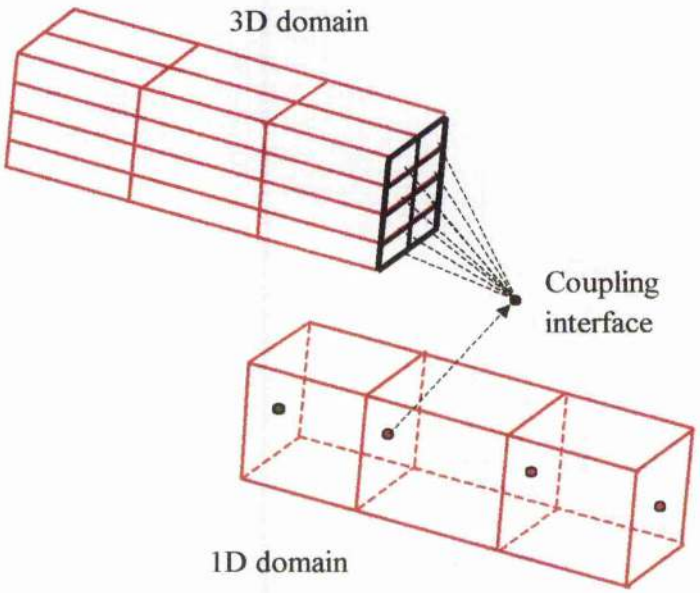

Figure 3-10: Overlap coupling: 1D to 3D information transfer

Figure 3-10 shows the flow information path from the 1D internal node to the boundary layer of the 3D domain at the end of the time interval. Due to the differencing technique adopted, conditions transferred to the 3D domain are those at the end of the time interval.

3.2.1.4 Fluid properties from 3D domain to 1D domain

Allowing the 1D and 3D domains to overlap, requires that the 1D boundary node information be obtained from inside the 3D flow domain. A control volume, defined inside the 3D flow domain, contains all of the fluid cells that are used in the averaging technique. Two methods of defining the control volume are discussed below.

3.2.1.5 Cell layer method

The cell layer method, defines a control volume over a single layer of fluid cells in the 3D flow domain. This cell layer stands at a distance equal to the grid spacing (Δx) from the boundary layer of the 3D domain. The method is demonstrated in the schematic of Figure 3-11.

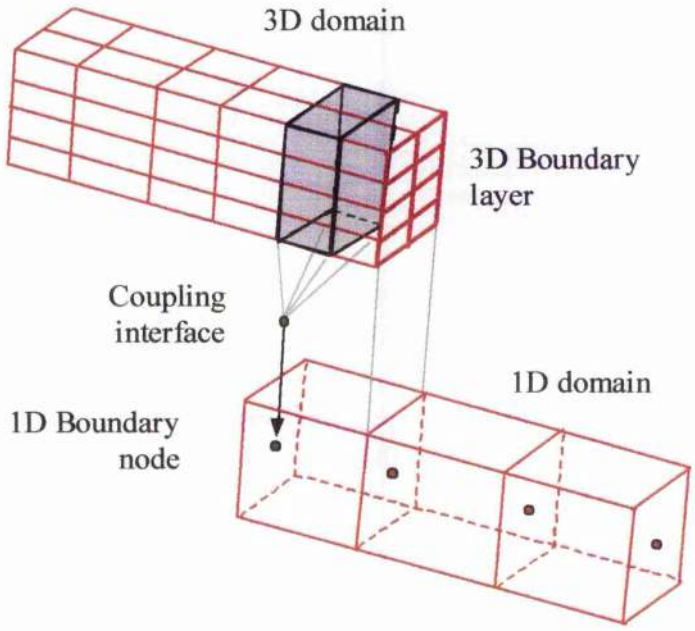

Figure 3-11: Overlap Coupling: Cell layer overlap coupling

The 3D flow domain is shown in the upper part of the schematic; the grey volume is the control volume. The averaging method employs cells in the control volume.

Cell layer overlapping has a major disadvantage: an exact cell layer definition cannot be secured if the overlapping 3D region is constructed on tetrahedral cells. The cells should be hexahedral or prism at least.

3.2.1.6 Cell volume method

The cell volume method is a variant of cell layer coupling that compensates difficulties encountered when applying the latter. A group of 3D fluid cells close to coupling interface provides data for the coupling calculation. Fig. 3-12 illustrates the principles.

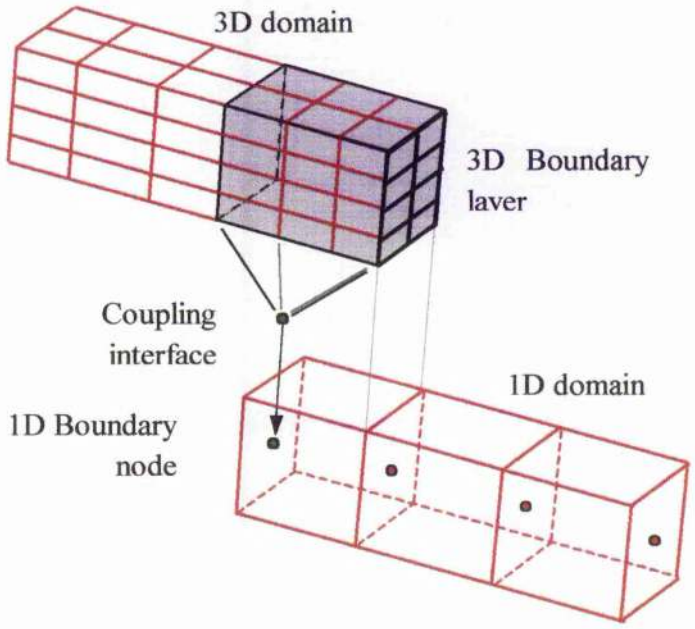

Figure 3-12: Overlap Coupling: Cell volume overlap coupling

A control volume spanning an entire cross section of the 3D flow domain is constructed. The control volume may include any number of cell layers up to a maximum corresponding to twice the 1D grid spacing. The sole criterion is that the centroid of the control volume shall coincide with the position of the 1D boundary node. Errors produced by including tetrahedral cells in the 3D flow domain are greatly reduced because a larger volume in implicated in the calculation.

3.2.2 Synchronisation

3.2.2.1 The Task

The synchronisation is of the implicit and explicit temporal discretisation schemes used by the 3D and 1D numerical methodologies. Figures 3-13 and 3-14 illustrate each of these schemes.

Implicit approach

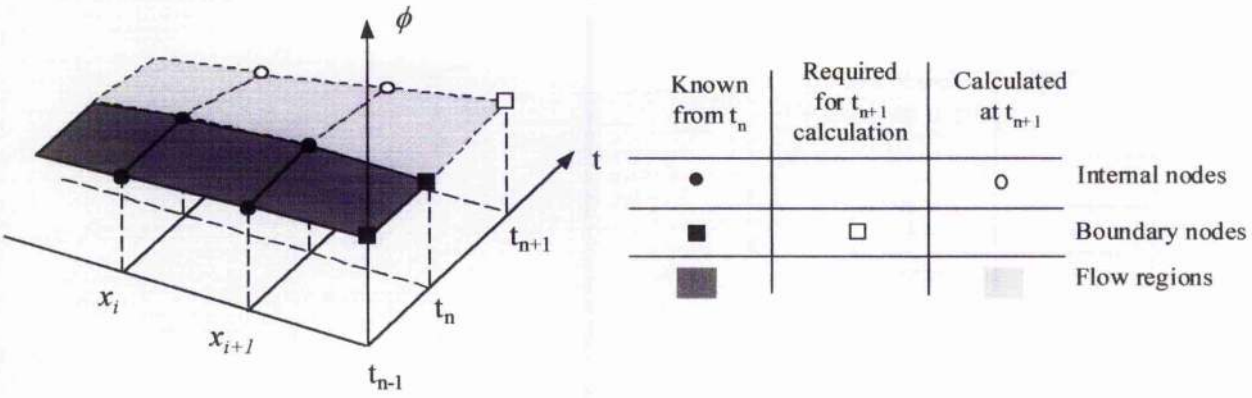

Figure 3-13: Time development with the implicit approach

Explicit approach

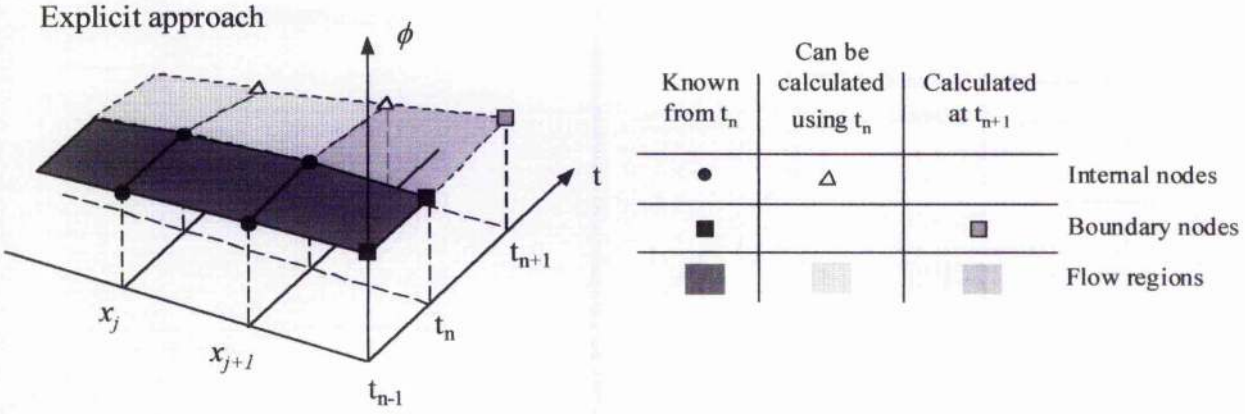

Figure 3-14: Time development with the explicit approach

Figure 3-13 defines the condition of an implicit numerical calculation at the end of a specific time interval. The nodes represent a mean fluid property over the cross section. At the end of time t_n the flow conditions are known at the internal nodes and on the boundary region. The implicit code requires that boundary conditions at the end of time t_{n+1} shall be determined before internal nodes can be calculated.

Figure 3-14 defines the condition of an explicit numerical calculation at the end of a specific time interval. At the end of time t_n flow conditions are known at the internal nodes and the

boundary region. The explicit code can compute on the internal nodes up to the end of time t_{n+1}. However, the boundary region of the explicit code cannot be computed unless the upstream flow is defined.

Consequently, the implicit and explicit schemes cannot exchange boundary conditions at time t_{n+1}. The following section will discuss two methods which will secure synchronisation.

3.2.2.2 Boundary Face Method

Figure 3-15 exemplifies synchronisation by the boundary face technique. For simplicity, the time step size assumed to be the same in the implicit and explicit calculations.

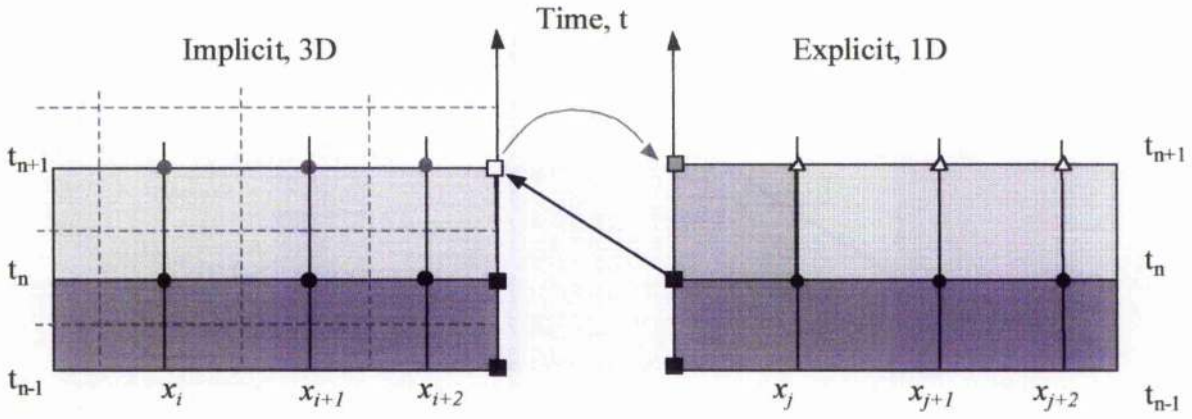

Figure 3-15: Schematic depicting the time at which information is exchanged with the boundary face method

Fluid flow properties are instantiated at t_n in all computational nodes of implicit and explicit schemes. The task is to provide the implicit scheme with boundary conditions at t_{n+1}, which latter is not by the explicit scheme.

The boundary face method transfers flow conditions from the explicit model corresponding to t_n, and applies them to the boundary region of the implicit flow domain at t_{n+1}. Thereby, the implicit method can proceed to calculate the internal flow up to time t_{n+1}. Data generated at the implicit (3D) boundary region and transferred to the explicit (1D) scheme, the latter is able to continue its determination of the field up to t_{n+1}.

The CFL criterion (section *4.1.2*) determines the maximum time step that the explicit method can accommodate. However, the implicit scheme is not so constrained; longer time intervals bring computational economy. Nonetheless, synchronisation demands control of the time step in both programs.

For clarity, the schematic Fig.3-16 impressed identical time steps on explicit and implicit schemes. However, the implicit code can compute on a longer interval and gain economy. Interpolation provides boundary conditions needed by the explicit code at shorter intervals.

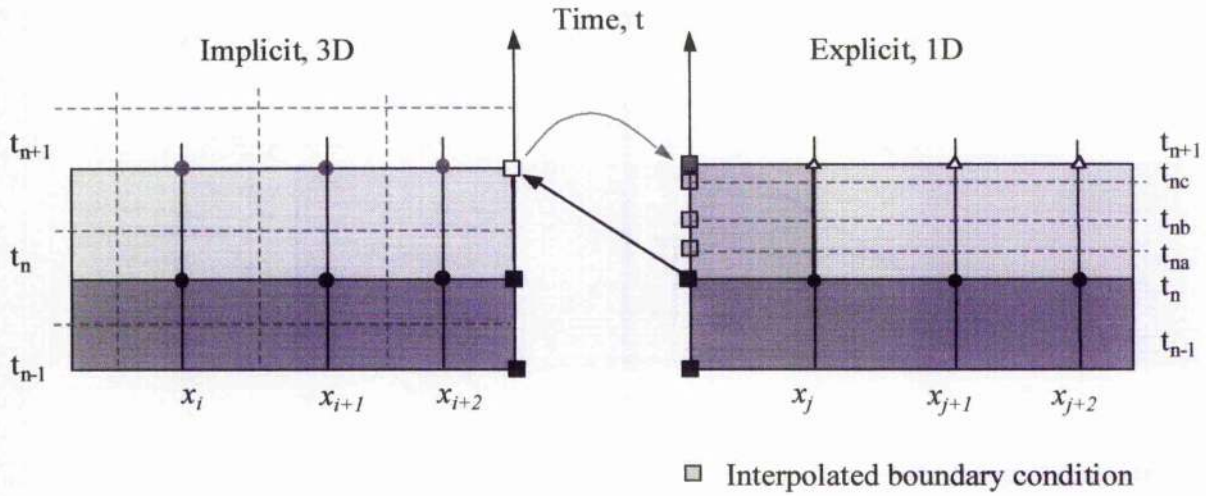

Figure 3-16: Schematic of the Interpolation process in the boundary face coupling interface

Interpolation between the old boundary conditions t_n and the new boundary values t_{n+1} is carried out when the time step used for the implicit calculations is larger than that used in the explicit code. Application of the interpolated boundary conditions t_{na}, t_{nb} and t_{nc} to the explicit code at intervals set by the stability criterion continue until the implicit code is ready to receive boundary conditions and conclude another cycle. Since boundary conditions for the 3D code correspond to the previous time interval, this method incorporates a discrepancy between the codes of one time step.

3.2.2.3 Overlap Method

Overlapping the 1D and 3D models rectifies this discrepancy of one time interval. Fig. 3-17 illustrates the effect: the implicit and explicit codes share a spatial interval.

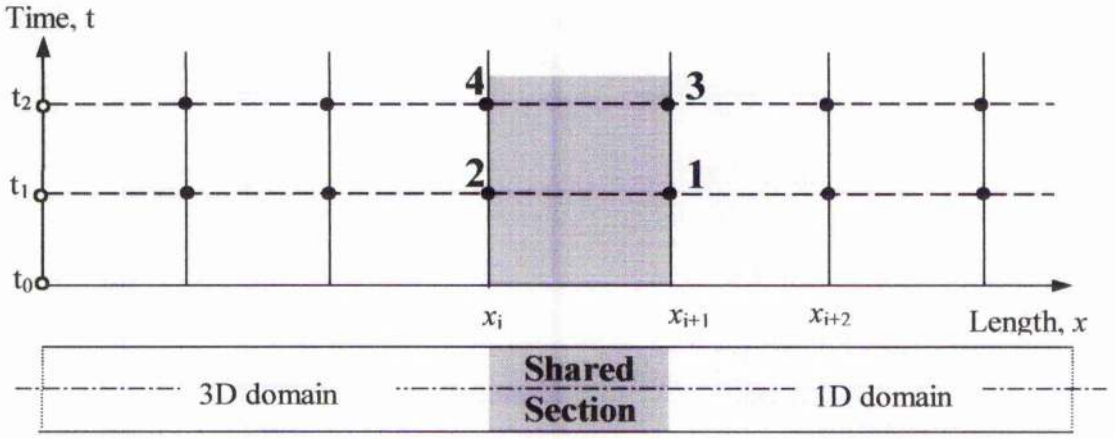

Figure 3-17: Schematic illustrating the shared section of geometry with the overlap coupling method

The explicit scheme requires the old time step t_n values in order to calculate the internal nodes at the new time step t_{n+1} [3]. The overlap method transfers these internal flow conditions to the implicit code as boundary conditions at the end of the time interval, t_n. After which the

implicit model calculates the internal flow and find fluid flow properties inside the 3D flow domain, represented as point **2** in the figure. The newly found values exchanged as boundary conditions with the explicit code, point **3**, the explicit code calculate the next time step. This procedure continues until completion, unless an error occurs.

The location at which fluid conditions are averaged in the implicit model must be specified before this overlap method can be implemented. The explicit approach requires three grid nodes (section *4.1.2*). The location of the averaging method inside the implicit model is defined by the spacing of the explicit grid: the distance $(x_{m+1} - x_m)$ is equal to $(x_{n+1} - x_n)$.

This overlap technique requires that explicit and implicit calculations share the same time interval. Interpolation being prevented, this method is computationally slower than is the boundary face method.

3.2.3 Efficacy and Efficiency

The overlap method suffers the disadvantage that the computational nodes may not lie at exactly the same distance from the boundary that the grid defined in the explicit code specifies. Values must then be found by interpolation between adjacent nodes or be taken from the nearest computational node. Furthermore, if the grid adopted in the implicit approach includes tetrahedral elements, the averaging method described previously (section *3.1.2.2*) is insufficient, for the nodes are not necessarily parallel to each other. In this case the cell volume overlap method (discussed in section *3.2.1.2*) is more appropriate, as more than one layer of cells is used in the interface calculations.

The boundary face method is uncomplicated, independently of the discretisation method used. However, it suffers the disadvantage that it leaves the codes asynchronous by one time interval. Nonetheless, the coupling scheme used this method. Therefore, the interface data exchange includes an extra parameter, the length of the time step. CFL criteria affect the 3D code, restricting the step size. The largest Courant number occurring in the entire 3D flow domain is related to an ideal Courant value promoted by the user, so that an ideal time step may be passed to the 1D code.

In summary:

	Boundary face method	Cell volume method
Cell type	*Hexahedral*	*Hexa & Tetrahedral*
Time synchronisation	*Single time step discrepancy*	*Codes synchronised but slower*
Execution	*Simple*	*Complex*

3.2.4 Interfaces Sited

Consideration must be given to the placement of interface between 3D and 1D regions. Parametric studies have revealed that the positioning of the interface is significant for stability (appendix C). Since the 1D method employs loss coefficients, the coupling interface is best placed at a location in the model where the fluid flow is essentially one-dimensional and explicitly is free from re-circulation. The consideration of boundary placement is best illustrated with the aid of a coupling example.

3.3 Initialising Hybrid Models

The choice of initial conditions greatly influences the run time and stability of the calculation required to reach a periodic state, from which an analysis can proceed.

The hybrid technique depends upon an individual initialisation of the codes. Given the high efficiency of the 1D code, its initialisation requires no more than that it be allowed to calculate a sufficient number of engine cycles to converge on a periodic state [17]. This 1D initialisation phase requires that the entire engine system be modelled one-dimensionally. Thereafter, the 3D model may run, initially using constant boundary conditions determined during the 1D initialisation. Constant boundary conditions are sustained until the 3D flow field reaches a steady state, signalled when conditions in cell layers neighbouring the boundary region remain unchanged.

Boundary conditions are best transferred to the 3D model during the initialisation procedure when spatial gradients in the boundary region are small.

The initialisation procedure follows this order:

- The 1D code calculates until it reaches a periodic state. At this stage, the 1D model includes the region modelled eventually using the 3D methodology.
- Boundary conditions are sent to the 3D code when the 1D calculation attains a periodic state.
- With boundary conditions held constant, the initialisation of the 3D calculation commences. The 1D code stands idle.
- The 3D calculation continues until convergence criteria are satisfied.
- The hybrid phase commences when notified that the 3D model is successfully initialised.

3.4 Recovery from Failures

A numerical calculation may. Cost considerations and computational efficiency require that calculations that stop unexpectedly, e.g. due to machine failures, be recovered to the state immediately prior to the failure. All information computed must therefore be saved at the conclusion of successive time steps.

Given the high speed of the 1D code it is sufficient to record the boundary conditions sent by the 3D code to the 1D code during coupled calculations. In the event that a computational failure occurs the 1D code can be restarted, with little loss of time, by reading the record of the 3D boundary conditions.

In comparison, the 3D code is computationally demanding. Therefore, all of the cell data in the 3D model should be kept at the end of a time step. However, outputting of the entire 3D data set constitutes a considerable computational effort. A compromise provides for this record to be written on receipt of a restart signal sent at pre-set intervals (i.e. every 10°CA). Thereby, the synchronicity of the 1D and 3D restart information is ensured at the small cost of re-calculating a few lost time steps.

3.5 Turbulence Modelling

Turbulence parameters are assigned to coupling interfaces at the start of every 3D time step. The choice is between specifying the turbulence quantities (i.e. k and ε) at the start of the calculation and to hold them constant thereafter, or to accommodate velocity changes by calculating new turbulence quantities at every time step.

The standard k-ε turbulence model, approximates k and ε using the following equations:

$$k = \frac{3}{2}\overline{u}_t\overline{u}_t \qquad \textit{Eq. 3.11}$$

$$\varepsilon = C_\mu^{\frac{3}{4}} \frac{k^{\frac{2}{3}}}{l} \qquad \textit{Eq. 3.12}$$

Where, $\overline{u}_t$ = turbulent intensity * velocity, and l = 0.07L where length L is a characteristic length i.e. the pipe diameter. The constant C_μ is defined in section 2.2.2.2.

The output of the 1D code yields the velocity. Therefore, new boundary values of k and ε can be found at the start of every 3D time step if the turbulent intensity is kept constant.

3.6 Programming Issues

Commercial codes permit limited access to the source code. However, sub-routines are available where additional code can be written to manage boundary conditions and values. A scheme for extraction of values from the numerical domain has been coded.

3.6.1 Communications

An aim of this study was to develop a universal coupling technique. Writing the necessary information to an external file facilitated data exchange between the 1D and 3D programs. Therefore, as long as the file format is defined, any numerical program may be coupled to any other related program. The opening and closing of files adds little to the computational time of the 3D numerical calculation. This transfer technique is independent of the platforms on which the programs are ported.

3.6.2 Control

The most important control is that applied to evaluations of the cross sectional area of the model at interfaces. Though the area definitions in 1D and 3D regimes may be satisfactory and complete, differences in the representations – in the cell structure – can create a mismatch of regional values that affects calculations of boundary conditions. Cell sizes at the boundaries must then be controlled and defined carefully. A check that matches the areas calculated on either side of the interface must precede every coupling calculation.

A boundary identification number must be exchanged to ensure that fluid properties are placed on the correct boundary region before the coupling calculation starts.

The practice calculates a large number of engine cycles by the 1D method (cycles of 720° crank angle), seeking a quasi-static solution at the chosen engine speed. Similarly with the hybrid scheme, a number of complete engine cycles must be computed before post processing may proceed. At least three engine cycles are required to ensure that spurious pressure waves have time to dissipate. Both codes must be signalled entering the last engine cycle, so that fluid properties can be saved for subsequent analysis.

4 EVALUATION OF INTERFACE MODELLING

4.1 The Model

A straight length of constant diameter pipe is analysed using the hybrid mode, i.e. with section of pipe modelled in three dimensions. This model was chosen because the flow within it cannot be in doubt.

Information transfer is analysed by comparing the hybrid model with an entirely 1D model of the pipe. The effects of increasing the time step on the coupling interface are examined with the purpose of evaluating the application of the stability criterion. An extension of the analysis examines the flow distribution model (vide chapter *3.1.3*).

4.2 Information Transfer

Figure 4-1 shows the division into three sections to provide flexibility in defining the hybrid model.

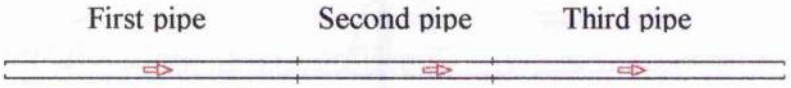

Figure 4-1: Schematic of straight pipe case

4.2.1 Numerical Arrangements

The pipe was initialised with a constant pressure throughout of 1.2b and with this same pressure held constant at the exit boundary. A pressure of 1.3b was applied at the inlet boundary, so that a pressure wave would propagate into the pipe.

4.3 The Simulation

Figure 4-2 describes the hybrid scheme; the centre section is modelled three dimensionally. The 3D meshing geometry was controlled carefully to secure conformance with the cross-section defined in the 1D representation.

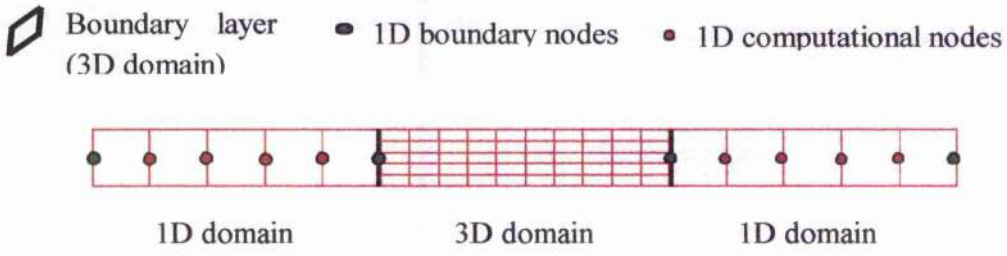

Figure 4-2: Straight pipe, hybrid model

4.3.1 Results

The comparison is of the hybrid scheme with a 1D representation. A pressure difference of 0.1 b was applied instantaneously across the pipe ends.

Figure 4-3 traces the propagation through the pipe of the ensuing pressure wave. The upper plot corresponds to the 1D reference model; the lower plot demonstrates the behaviour of hybrid model. These traces were plotted using the 1D code post-processor; the results of the 3D section of the hybrid model are, perforce, omitted.

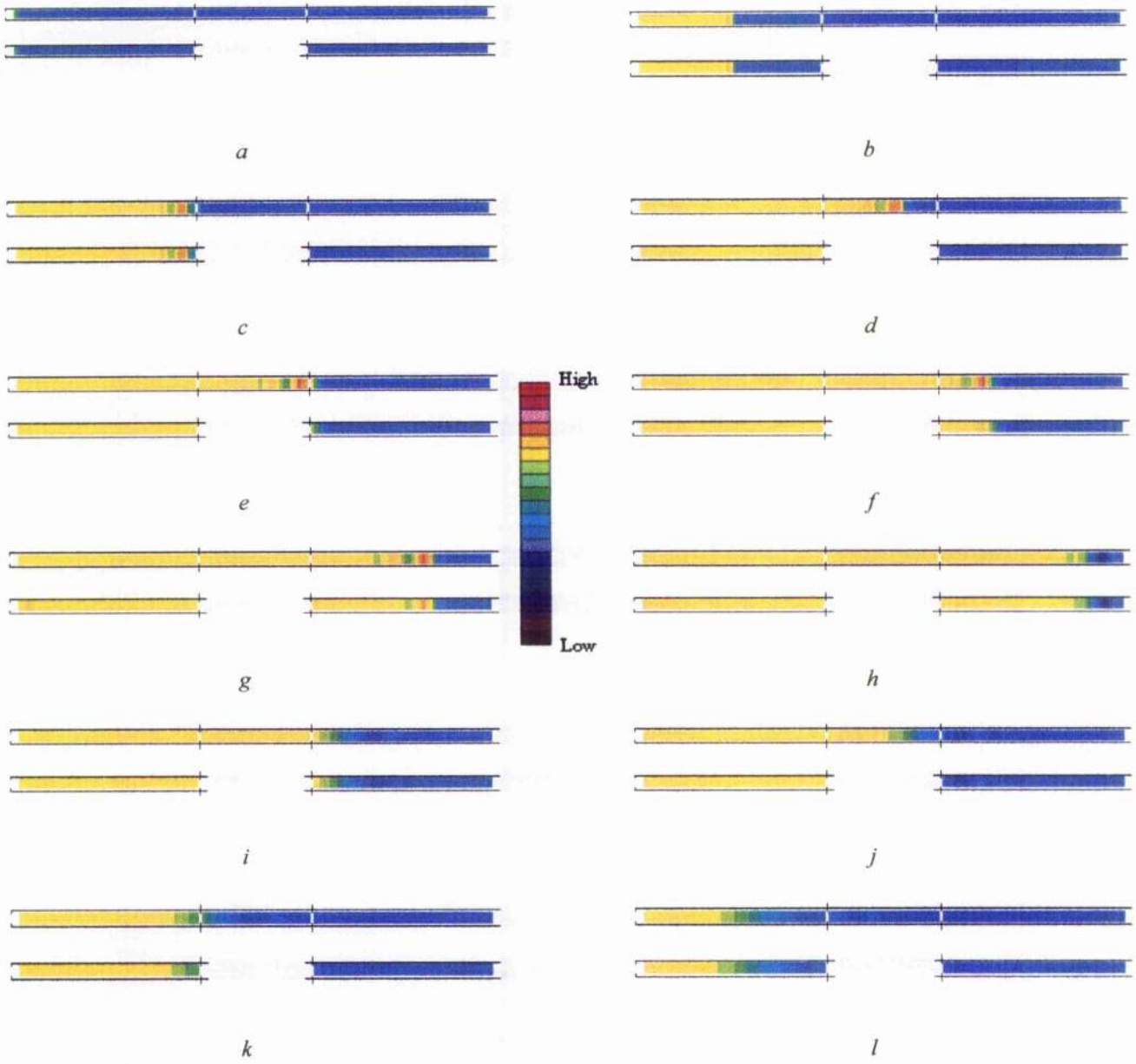

Figure 4-3: Pressure wave transport through 1D and hybrid model

The 1D and hybrid model have identical start conditions (*a*). The first coupling interface of the hybrid model does not generate reflections. The models predict the same flows, passing through the second pipe. Figures (*f*) through (*k*) trace the wave propagating in the third pipe. Due to the prescribed constant pressure boundary condition applied to the end of the third pipe, the wave incident is reflected consistently. This reflection, passing upstream and entering the second pipe (*l*) (Modelled in 3D), not reflected into the third pipe by the coupling interface.

These several results confirm the integrity of the coupling scheme: the interface is evidently transparent, for it does not generate spurious reflections.

4.4 Velocity Profiles Inferred at Entry to 3D Regions

The straight pipe is an ideal case for assessing the profile methodology (vide section *3.1.3*). Empirical data is secure for this case and detailed mathematical models offer proven predictions. The test is of the capacity of the three dimensional section of the pipe model to predict the form of the developing transverse velocity profile. The calculations reported above produced non-uniform, radial velocity profiles in the exit plane of the 3D modelled pipe, as might be expected from a model that admits turbulence. The demonstration sought here is that the interface is robust in its support of the scheme that applies a velocity profile to a 3D region that is inferred from 1D data.

4.4.1 Block Profile and Inferred Profile Cases Compared

Figures 4-4 and 4-5 illustrate turbulence in a 3D modelled region affecting an initially block velocity profile.

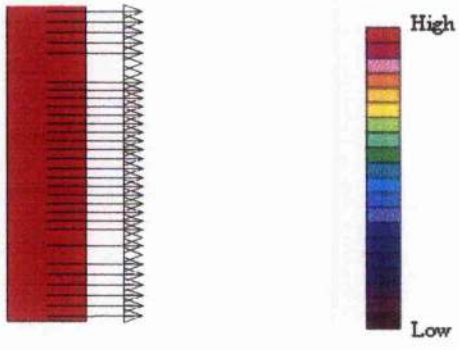

Figure 4-4: Inlet cell layer, impressing a block profile

Figure 4-5: Outlet cell layer: Turbulence affecting a block velocity profile.

The arrows in the above figures are velocity vectors. Given the shortness of the 3D pipe model segment, the outlet profile is little affected by wall effects. Nonetheless, the development of a boundary layer is evident.

Figures *6-6* and *6-7* demonstrate the application of the profile inference technique.

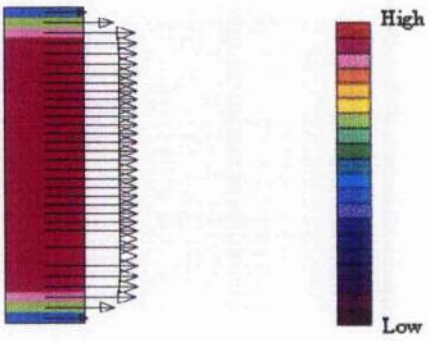

Figure 4-6: Inlet cell layer, impressing an inferred velocity profile on the boundary

Figure 4-7: Outlet cell layer, demonstrating development of the inferred input profile.

Turbulence in the 3D region has greatly amplified the boundary layer that was impressed at the interface of 1D and 3D regions.

4.5 Results Summarised

Calculations that predict transient flows in a straight pipe have tested the efficacy and robustness of the coupling scheme which controls interfaces in hybrid models. The first criterion, that interfaces shall not generate spurious reflections, is satisfied. Interfaces are transparent to downstream and upstream propagating waves. The second criterion, that the interface shall remain transparent when subjected to velocity profiles inferred from 1D data, is satisfied. The growth of a boundary layer impressed on the input plane of a 3D modelled region is rapid. This technique of inference is a powerful and essential aid to the accuracy of hybrid modelling.

5 AUDI V6 TDI

5.1 Introduction

An industrial scale application of the hybrid methodology, demonstrated herein, analyses the charge air pipe of a current Audi diesel engine. Designed for compactness, this pipe system contains elements in which the flow is essentially three-dimensional.

A brief description of the Audi engine is proffered; a detailed description of the inlet pipe identifies regions that affect engine performance. Though this work does not set out to prove the 1D technique, the results of 1D and 3D calculations are compared to those derived from engine bench tests.

5.2 Engine Description

Audi [43] introduced its 2.5l V6 TDI engine to the automobile market late in the last century. Figure 5-1 depicts the TDI engine, which is rated at 110 kW and delivers a maximum torque of 310 Nm. The data given in the table below characterises the engine.

Main engine data

Stroke	86.4	mm
Bore	78.3	mm
Connecting rod length	158	mm
Volumetric piston displacement	2496	cm^3
Firing order	1-4-3-6-2-5	
Compression ratio	19.5:1	
Rated capacity at 4000 rpm	110	kW
Maximum torque at 1750 rpm	310	Nm

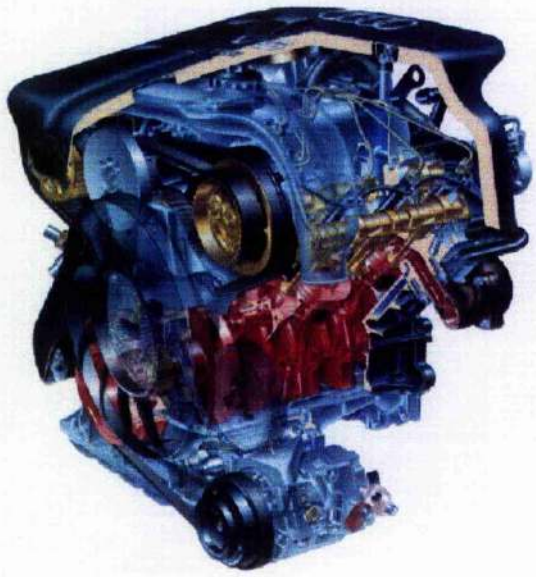

Figure 5-1: The Audi V6 TDI

Figure 5-2: Charge air pipe of the V6 TDI engine

The charge air pipe supplies air to two cylinder banks; it is shown in Fig. 5-1as a transparent part, standing beneath the design jacket of the engine and above the camshaft of cylinder bank two.

Figure 5-2 illustrates the internal volume of the charge air pipe. The large cross-sectional area on the left hand side of the figure is the air inlet. Thereafter, the airflow bifurcates: one stream leads to cylinder bank one (far right), the second to cylinder bank two (larger of the two middle pipes). Exhaust gas re-circulates via the small (EGR) pipe in the centre of the figure. In this prediction of flow in the charge air pipe the EGR pipe remains closed.

5.3 Purpose and Aim

Figure 5-3 details the charge air pipe of the V6 TDI engine. Arrows in the figure define the direction of the airflow, leaving the charge pipe. Thereafter the inlet flow splits to provide separate airflows to the cylinder banks. The pipe that connects the split ports is a critical design feature; the volumetric efficiency of the engine depends upon this connection [44].

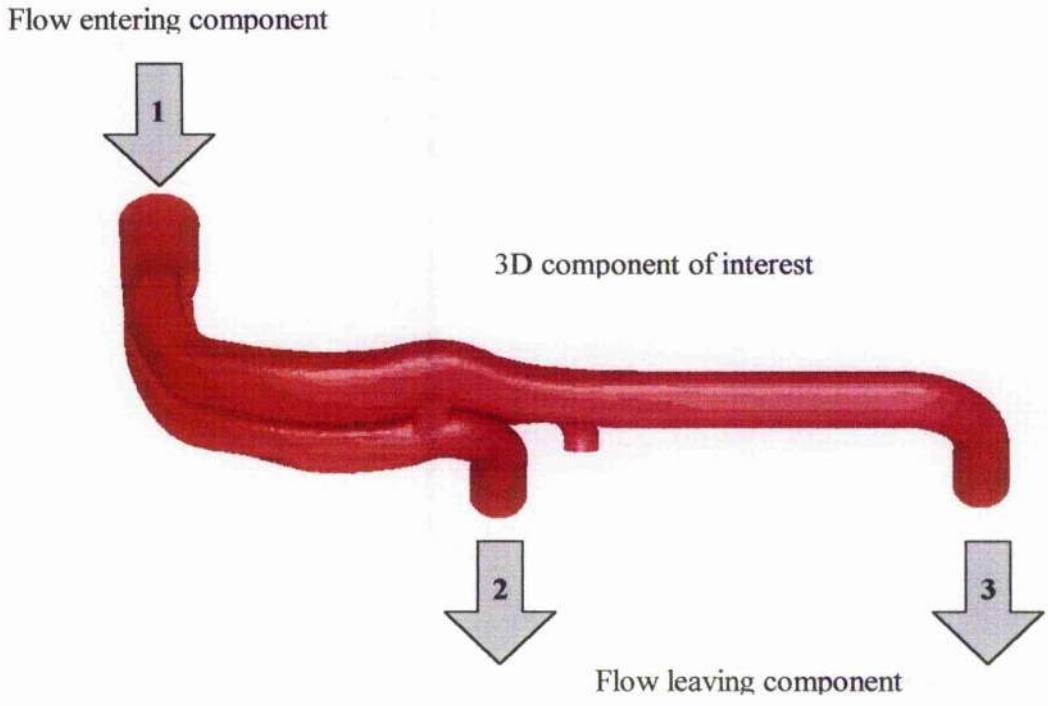

Figure 5-3: Charge air pipe, detail

Measurements alone are insufficient to produce a clear picture of flow effects inside the charge air pipe. An extensive mapping of the flow by LDA (Laser Doppler Anemometry, [46]) might suffice, but this technique is complex and costly. Therefore, the aim of the numerical analysis is to predict the effects of the connection pipe on the volumetric efficiency of the V6 TDI engine.

The volumetric efficiency is the ratio of volume flow rate of air into the intake system to the net volumetric rate displaced by the pistons [16].

$$\eta_v = \frac{\int_{Iv_o}^{Iv_c} \dot{m}_a dt}{\frac{p_e \cdot V_c}{R \cdot T_e}} \qquad \textit{Eq. 5.1}$$

The volumetric efficiency measures the capacity of an engine to breathe and, therefore, the success of the engine designer. It is easily measured [44].

Many factors influence the volumetric efficiency. The efficiency of cylinder charging is a function of the engine's rotational speed (time available to fill cylinder), the temporal variation of the pressure ratio across the poppet valves in the cylinder head, the geometry of the inlet manifold imposing pressure losses, and etc. Valve timing is an important factor and, related to this, the design of the exhaust system affects the scavenging of products of combustion from the cylinders.

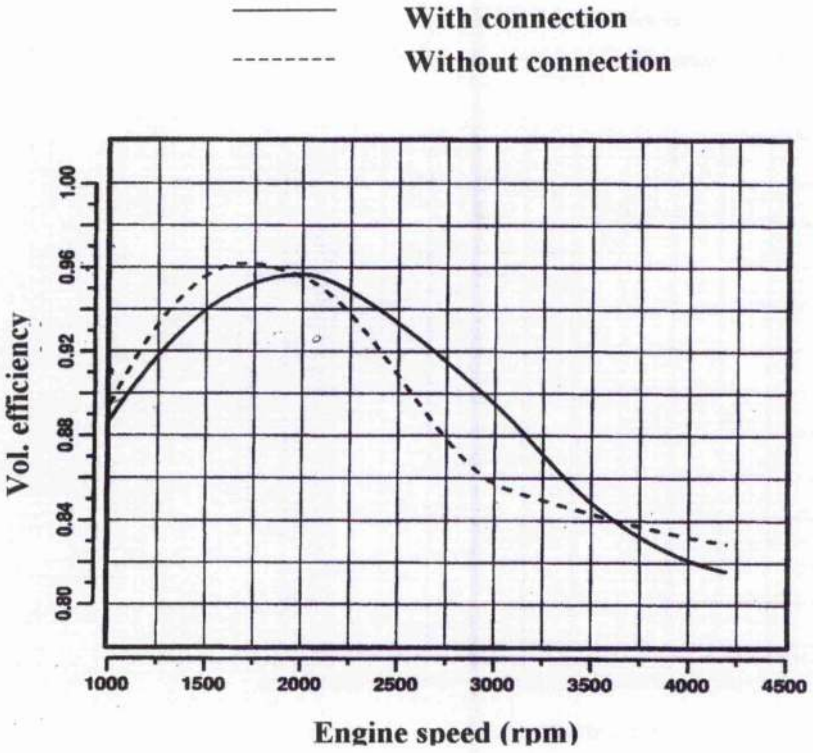

Figure 5-4: Volumetric efficiency of the V6 engine for different connection pipe configurations

Experimental data plotted in Fig. 5-4 demonstrates the effect of the inter-connecting pipe on the volumetric efficiency of the V6 engine. The inter-connection raises the volumetric efficiency significantly at engine speeds above 2000 rpm and up to around 3500/4000. An explanation for this enhancement of the flow is sought herein, through a numerical analysis of airflow in the engine at speeds between 2000 and 4000 rpm.

5.4 Predictions of Engine Performance

5.4.1 One-dimensional Prediction

5.4.1.1 Model described

A 1D model constructed reproduced the geometry defined in technical drawings of the engine accurately. The test bench engine yielded additional geometrical information.

Fig. 5-5 identifies the cylinder banks and turbocharger, including the latter's compressor and turbine. The inlet system and the inter-connecting pipe, being the components of interest, are positioned directly above the left cylinder bank (shown inside the dashed lines). The charge air pipe is regarded as being constituted from pipes and pipe junctions, so that the analysis can account for the interactions of waves propagating along the pipes at finite velocities.

Numbered diamond shapes identify locations at which experimental measurements were taken during bench tests. Flow conditions calculated at these locations (i.e. pressure, temperature, speed of sound, etc.) were saved for comparison with the experimental values.

5.4.1.2 Charge air pipe defined

As stated in [3], the loss coefficients required by the 1D model at a junction of two pipes differ depending upon the directions of flows in the pipes and vary according to the ratio of the mass flows exiting and entering the junction. A three-way junction can sustain six different flow configurations. In addition, an infinite number of mass fluxes can flow through each pipe for each of these six flow configurations. The 1D methodology requires that eleven different loss coefficients be determined for each individual flow configuration. Therefore, the calibration of the 1D model requires that sixty-six loss coefficients be determined.

Measurements of the cyclical flow were taken at increments of 500 rpm over a speed range from 1500 to 4400 rpm at the locations denoted by diamonds marked 1 and 2 in Fig. 5-5. These comprehensive experiments aided the definition of the numerous loss coefficients required by the 1D code.

Accurate modelling of the turbocharger posed a significant problem. The turbocharger has adjustable vanes [20] so a performance map must be constructed for every vane setting [21].

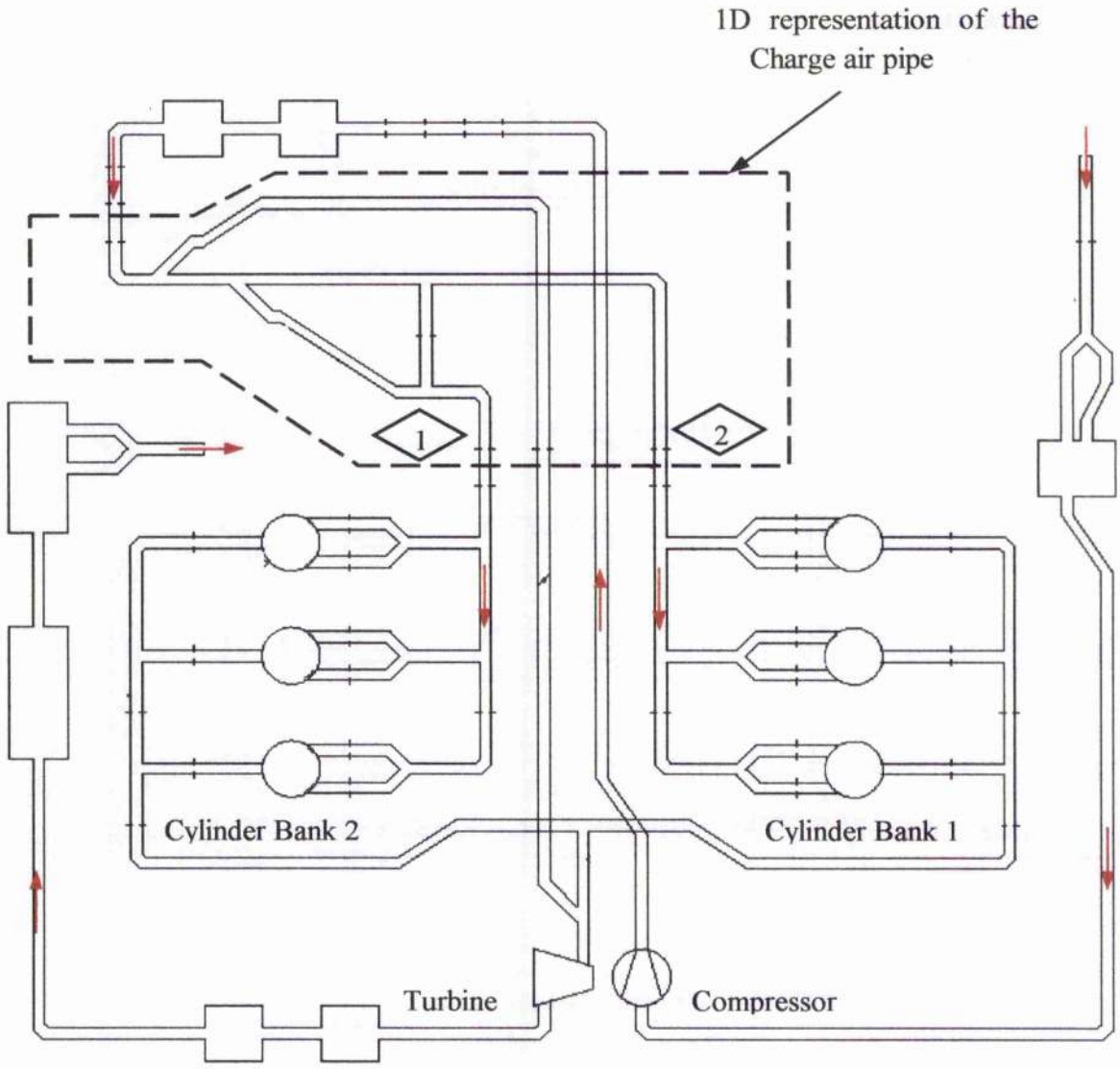

Figure 5-5: Schematic of the 1D model of the V6 TDI engine

5.4.1.3 One-Dimensional Prediction

The graph of Fig. 5-6 plots calculated values of the volumetric efficiency of the V6 engine and demonstrates the influence of the connecting pipe. Each point on the graph represents an individual 1D calculation. The cost of a smoother curve was unsustainable. Nonetheless, the predicted results coincide well with the experimental results given in Fig. 5-4. The experimental results should agree with the 1D analytical predictions, for the latter depended upon loss coefficients derived from the experimental data. However, these results prove that the 1D calculation predicts transport times correctly.

The greater slope of the unconnected pipe model is observed in both the experimental and calculated results. The improvement introduced by the connecting pipe is greatest at 3000 rpm, in the predicted and experimental results.

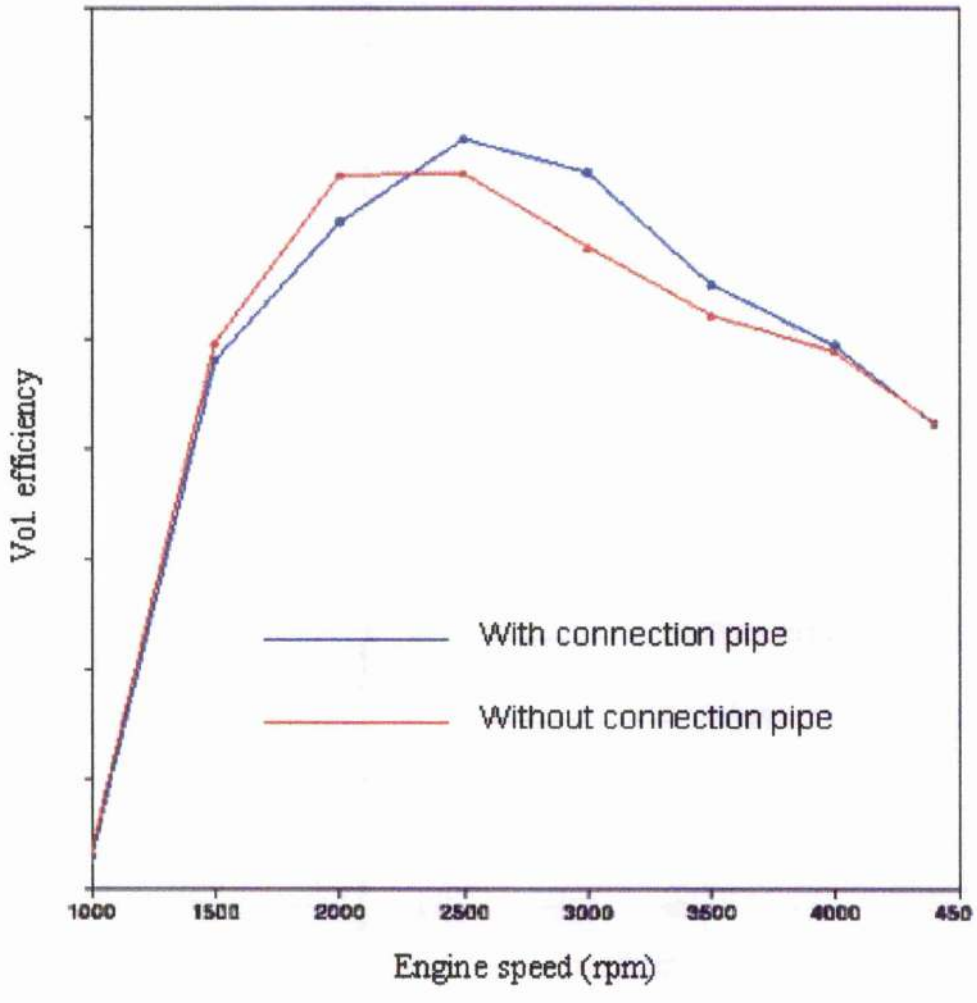

Figure 5-6: 1D modelling of the volumetric efficiency.

Figures 5-7 and 5-8 compare the predicted and measured pressures at two locations in the charge air pipe.

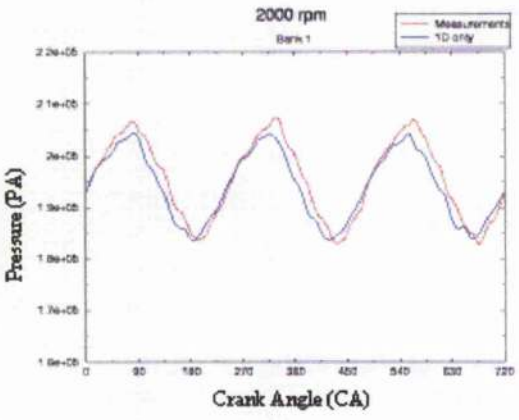

Figure 5-7: 1D results for bank 1 at 2000 rpm

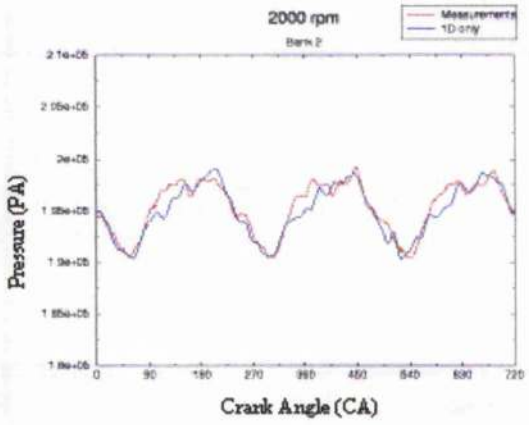

Figure 5-8: 1D results for bank 2 at 2000 rpm

Results are given for an engine speed of 2000 rpm alone, for this work does not aim to prove the accuracy of the 1D methodology. The original experimental work commissioned by Audi discharged this task. The sets of results plotted correspond to sites numbered 1 and 2 in Fig. 5-5. The numerical analysis closely reproduces the measured amplitudes and, signally, the phases of pressure waves.

These results demonstrate the accuracy of the 1D method when experimentally determined loss coefficients are available. When calculation time and accuracy are of vitally important, the 1D methodology is paramount in industrial practice.

5.4.2 Hybrid Model Prediction

A 3D model that could be interfaced with the 1D global model was constructed to investigate the flow field inside the charge-air pipe. The coupling methodology applies the transient effects predicted by the 1D model to the 3D model of the charge air pipe.

Since the 3D model evaluates losses in the connection pipe with the aid of turbulence modelling techniques, the 1D calculation can proceed without the benefit of experimental coefficients for this component.

5.4.2.1 Model Described

The global 1D model was unchanged, save for the removal of the charge air pipe.

The Motor Development Department of Audi, Ingolstadt contributed a CAD rendered surface representation of the charge air pipe, suitable for conversion to a volume representation. Discretisation of the volume in the manifold used SAMM (Semi Automatic Meshing Methodology), an Adapco software product. The volume meshes so generated were predominately hexahedral; near-wall mesh layers were constructed on 'Prism cells'. These forms in near-wall layers lent accuracy to numerical calculation in boundary layer regions. Guided by experience within Volkswagen, and allowing a pay-off between the computational time and accuracy, the model employed about 400,000 mesh elements.

Prior to the application of the boundary conditions, quality checks that assured the connectivity (sic) of the mesh, i.e. ensured that the mesh was 'hole' free and that cells joined face-to-face with vertices coincident. The preferences adopted for numerical mesh validation applied ERCOFTAC principles [47].

Figure 5-9 illustrates the hybrid model and, expressly, shows the 3D charge air pipe connected within the 1D model. The coupling methodology applied at the single inlet and twin outlet regions of the air charge pipe set the boundary conditions to the left and right.

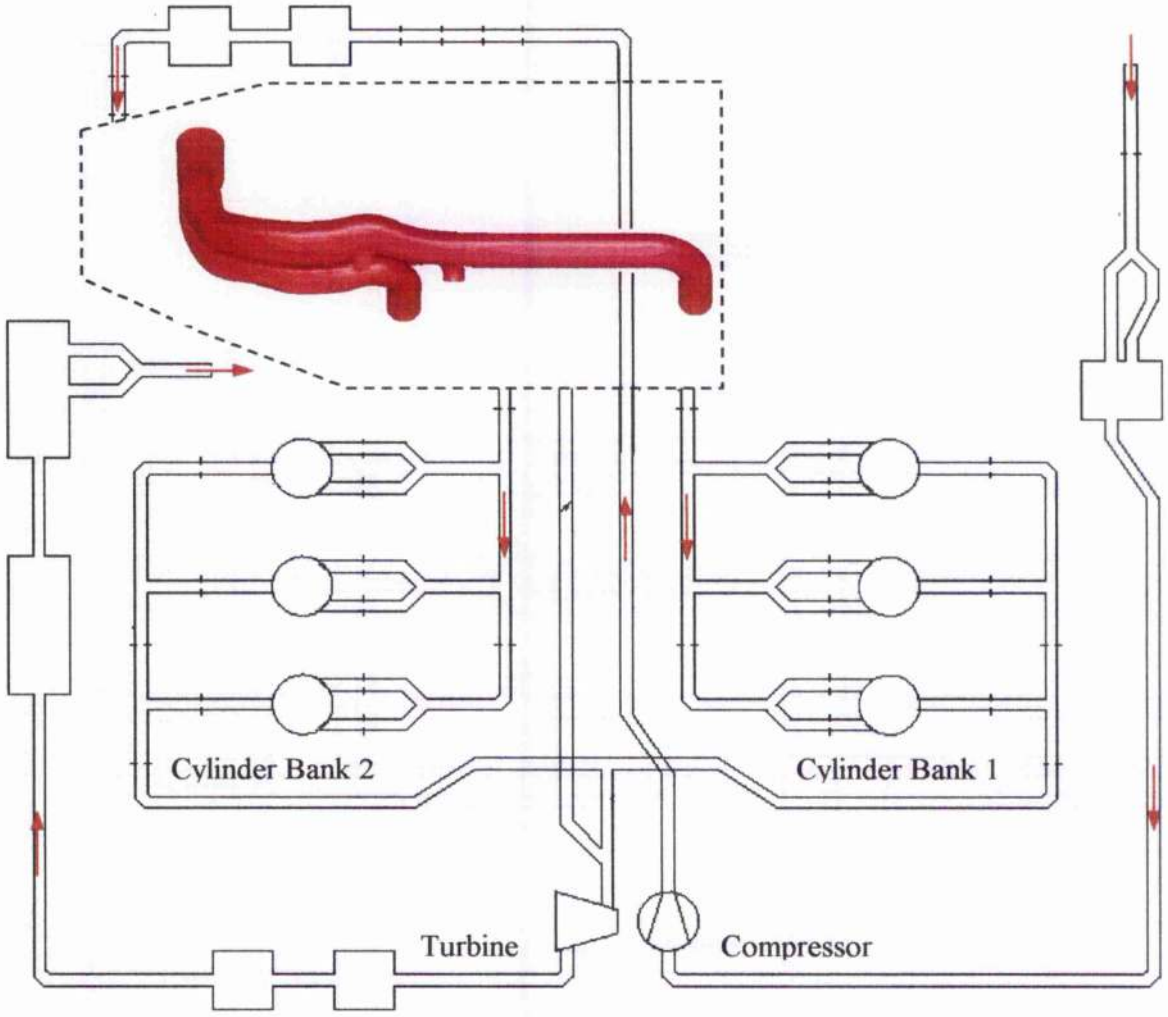

Figure 5-9: Hybrid model of the V6 engine

5.4.2.2 Three-Dimensional Prediction

The 1D results given previously and flows predicted by the hybrid model are compared here for three different engine speeds, viz 2000 rpm, 3000 rpm and 4000 rpm. The aim was to understand why the volumetric efficiency varied so strongly with engine speed (refer to Fig. 5-4). Further to the flow field analysis, pressure distributions are compared to measurements at locations corresponding to the diamond boxed numbers 1 and 2 of Fig. 5-5.

Figure 5-10 presents hybrid model predictions of the variation of volumetric efficiency with the engine speed. Hybrid results are plotted coincidentally with the results of 1D calculations. Small discrepancies between the 1D and hybrid numerical methods are evident at all engine speeds. The largest difference occurs at 2000 rpm. The next section discusses the phenomenon that may be responsible for this result. The smaller differences evident in volumetric efficiency predictions calculated by the 3D model imply that this model is better able to predict losses.

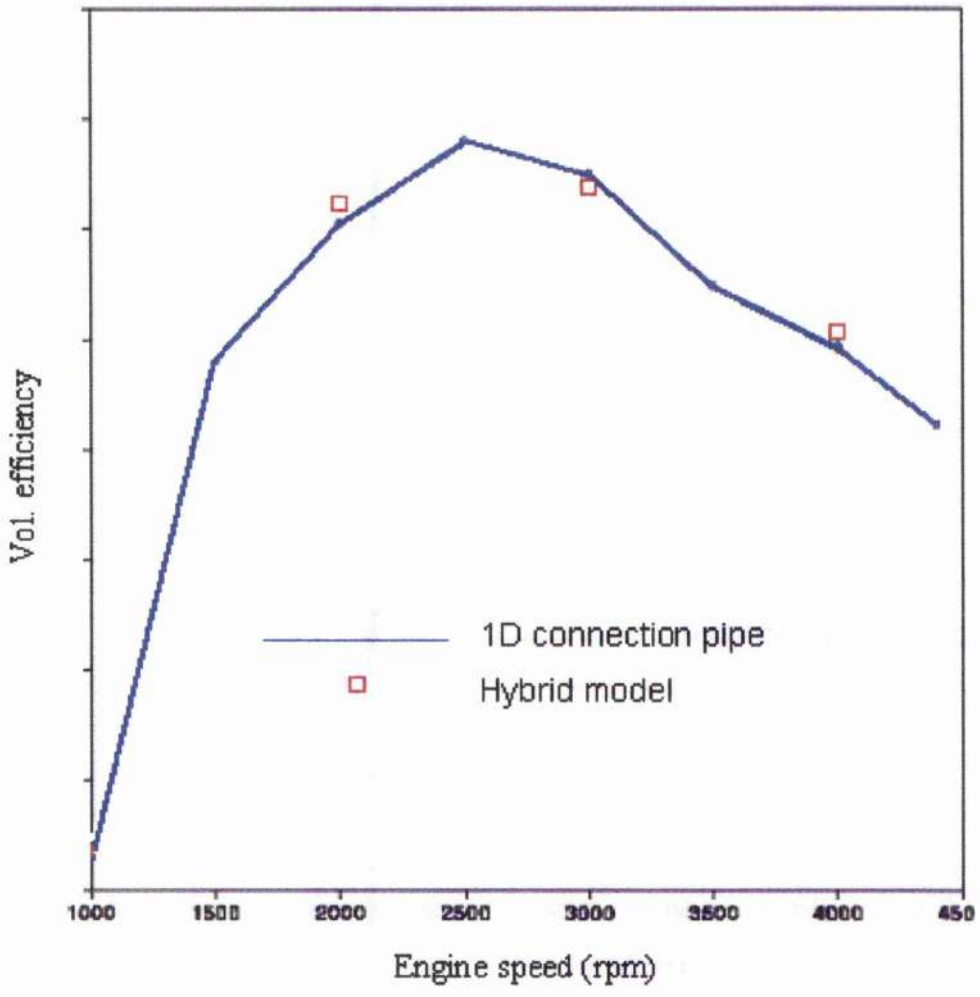

Figure 5-10: Volumetric efficiency results of the Hybrid model

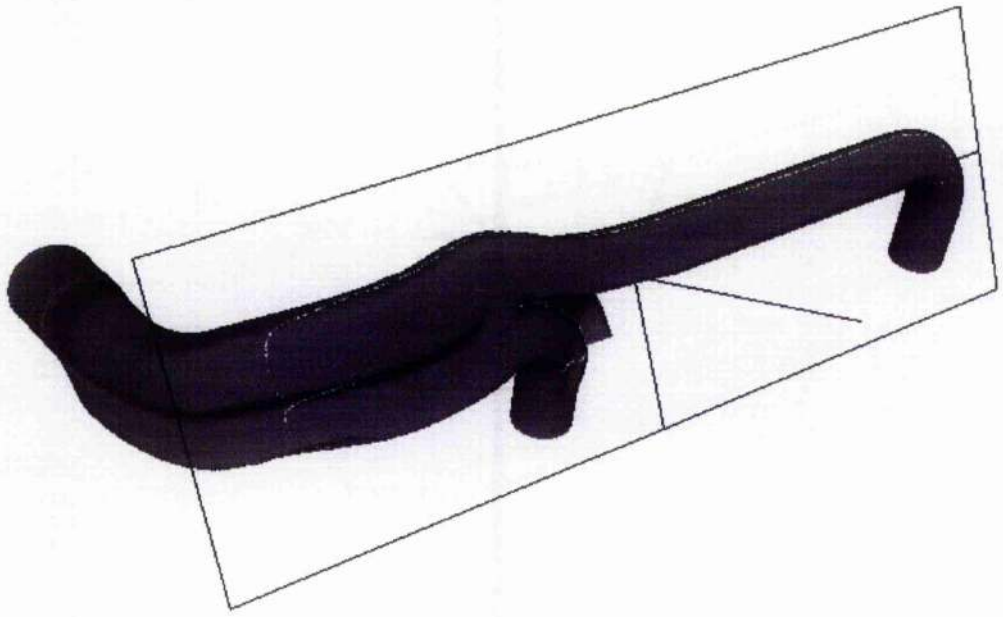

Figure 5-11: Intersection of the reference plane with the charge air pipe.

The flow field is analysed using a vector plot technique: arrows projected on to a two-dimensional plane define the direction of the flow; they are colour-coded according to the magnitude of the velocity. The plane incorporates the pipes leading to banks 1 and 2 and reveals the flow field in the connection pipe completely. Figure 5-11 locates the two-dimensional plane within the charge air pipe.

Case 1: 2000 rpm

Figure 5-12 compares the computed results (black curve) and experimental measurements (red curve) of the pressure, the latter taken from cylinder bank 1 of the test bench engine. The curves extend over a complete engine cycle of 720 degrees crank angle. Three peaks that coincide with the closure of an inlet valve in the cylinder bank are evident. Minima on the plots correspond to crank angles at which the inlet valves are fully open. These manifestations of complex gas exchange process in play during an engine cycle are reproduced by the computational prediction. Inlet valve movements determine the recorded pressure waves, since the pressure transducer is sited remotely from the connection pipe.

The transducer for cylinder bank 2 is located closely to the connection pipe, where the effects of valve closures are less evident. Pressure waves recorded are consequences of 3D form oscillations within the connection pipe. The predicted temporal variation of pressure plotted in Fig. 5-13 reproduces these oscillations.

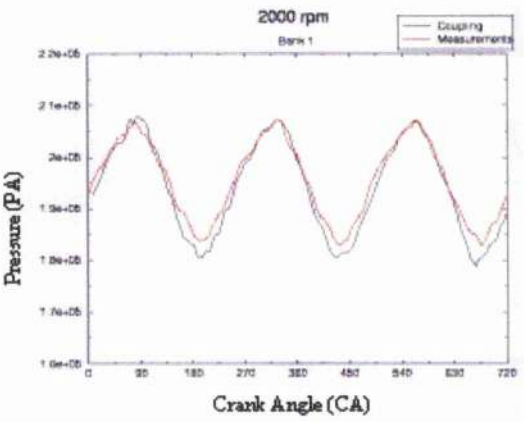

Figure 5-12: Bank 1 results at 2000 rpm

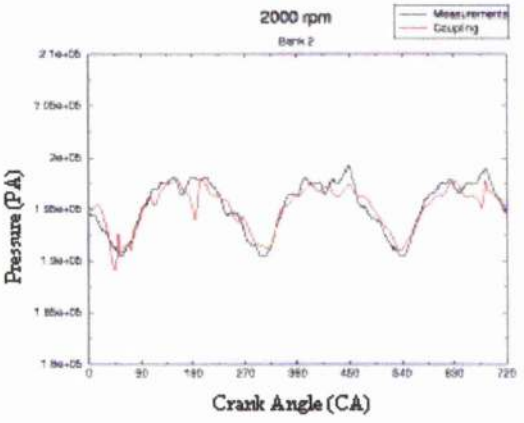

Figure 5-13: Bank 2 results at 2000 rpm

The following plots record the predicted velocity distributions projected onto the two-dimensional plane defined in Fig 5-9. The schematics offered on the right-hand side capture the primary flow characteristics. The consecutive plots are ordered according to crank angle.

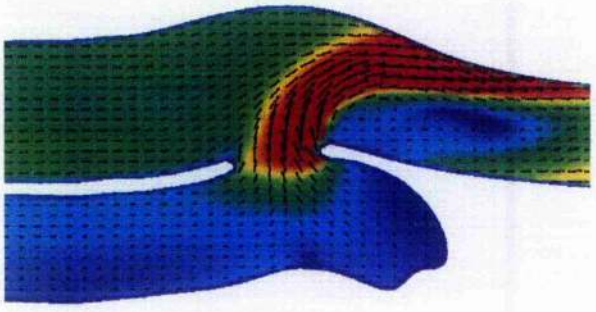

Figure 5-14: Flow to bank 1 at 2000 rpm

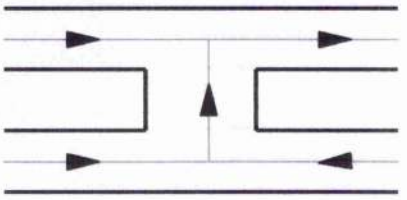

Figure 5-15: Schematic of bank 1 flow field

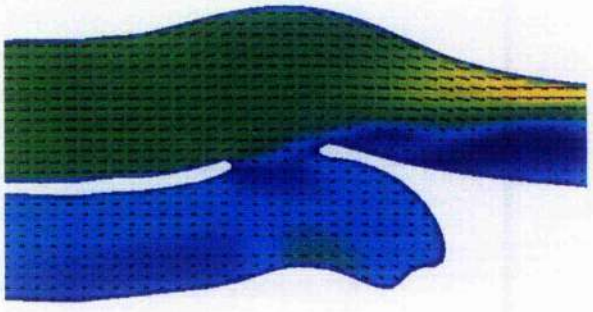

Figure 5-16: No flow through connection pipe

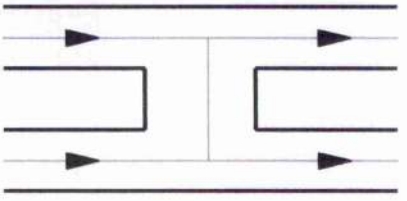

Figure 5-17: Schematic of no flow through connection pipe

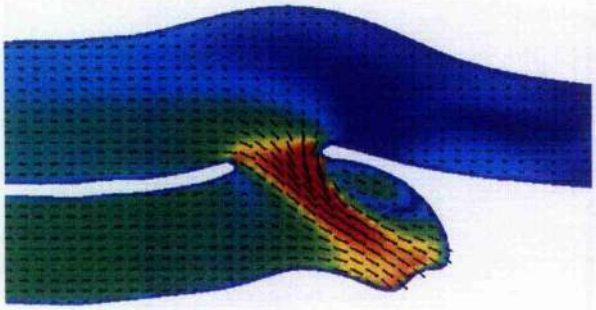

Figure 5-18: Upstream flow through connection pipe

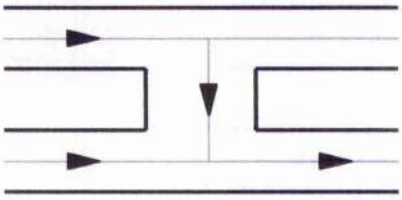

Figure 5-19: Schematic to upstream flow

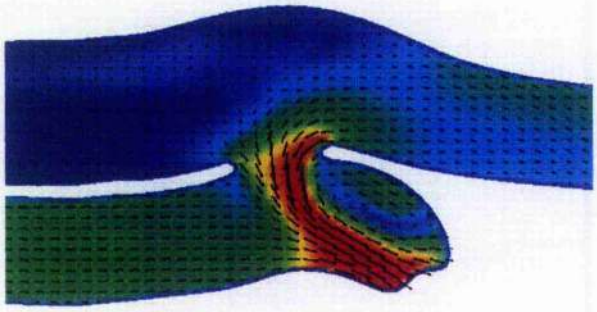

Figure 5-20: Downstream flow through connection

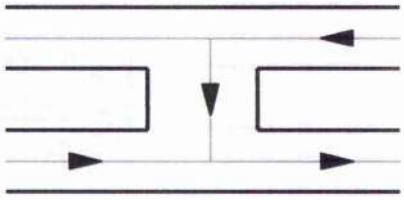

Figure 5-21: Schematic to downstream flow

The flow field shown in Fig. 5-14 represents the computational result as an inlet valve of a cylinder in bank 1 opens. Air enters bank 1 from upstream of the connection pipe and is received from bank 2. This air from bank 2 passes through the connection pipe from upstream and downstream directions (illustrated schematically in Fig. 5-15). Figure 5-16 shows the field as the valve closes in the bank 1 cylinder. Air passes above and below but not through the connection pipe. Figure 5-18 shows the flow field when an inlet valve to a bank 2 cylinder opens. Air enters bank 2 from upstream of the connection pipe and through the connection pipe. At this time, air passes through from the upstream direction alone (illustrated in Fig. 5-19). Figure 5-20 shows air passing through the connection pipe from the downstream direction. The corresponding schematic diagram, Fig. 5-21, depicts the flow field at this crank angle.

Flow entering cylinder bank 2 from upstream and downstream of the connection pipe (Figs. 5-18 and 5-19), causes reduced amplitudes found in bank 2 (Fig. 5-13).

The complex flow structure described above for the 2000 rpm engine speed contributes to the large differences observed between the 1D and hybrid calculations in the volumetric efficiency graph presented earlier (Fig. 5-4).

Case 2: 3000 rpm

Figure 5-22 shows the change of pressure with crank angle in cylinder bank 1 at an engine speed of 3000 rpm. Opening and closing of the inlet valves generates three pressure waves

evident in the graph. Due to the increasing engine speed, the amplitudes of the predicted and measured pressure waves present in bank 1 differ slightly; the amplitudes are somewhat greater than at 2000 rpm.

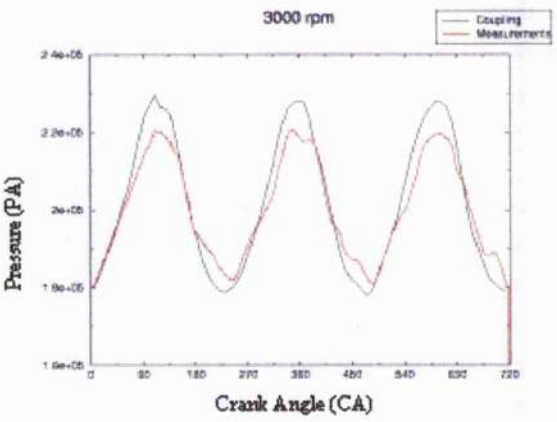

Figure 5-22: Bank 1 at 3000 rpm

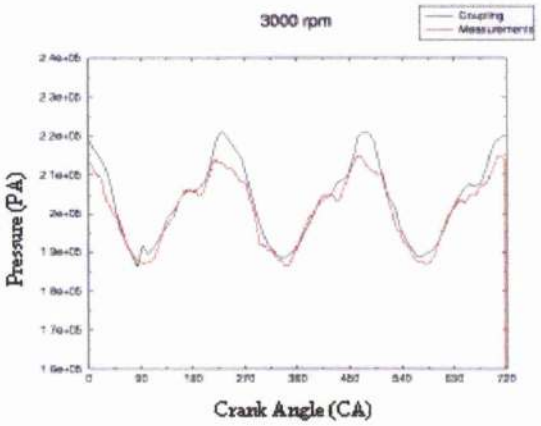

Figure 5-23: Bank 2 at 3000 rpm

Figure 5-23 shows that the opening and closing of inlet valves in bank 2 creates the primary pressure waves. High frequency oscillations are more in evidence. The two curves lie close together, so the hybrid prediction reproduces the primary characteristics of the experimental results. Comparing the pressure curve shown for bank 2 at 3000 rpm with those presented in Fig. 5-13 for 2000 rpm, there appear to be fewer higher-order, overlaid pressure waves. Furthermore, a phase shift has occurred in the pressure waves in both cylinder banks. The curves have moved through a crank angle of about 45 degrees compared to the 2000-rpm result.

The flow of air passing through the connection pipe is affected by pressure waves present in inlet pipes to both cylinder banks. This phenomenon will adversely influence the mass flow into both cylinder banks and thereby reduce the engine's overall volumetric efficiency.

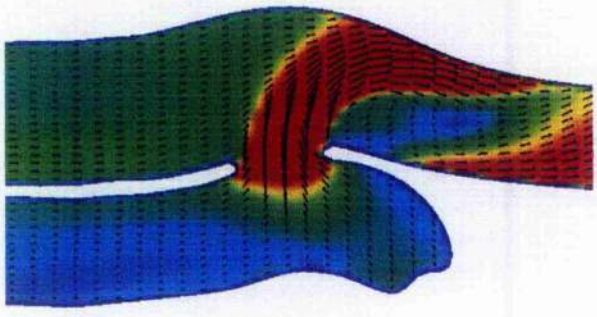

Figure 5-24: Flow to bank 1 at 3000 rpm

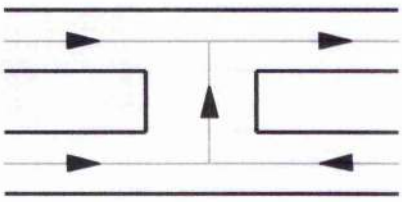

Figure 5-25: Schematic of bank 1 flow

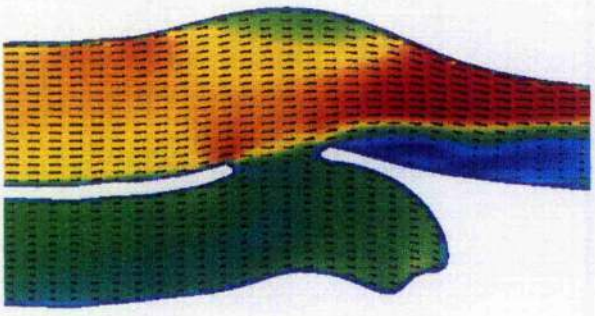

Figure 5-26: No flow through connection pipe

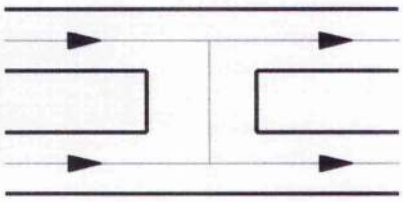

Figure 5-27: Schematic of no flow through connection pipe

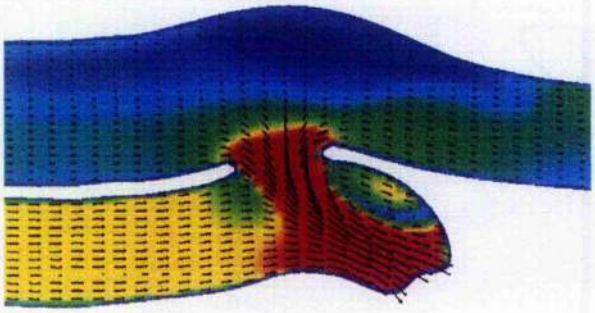

Figure 5-28: Bank 2 flow

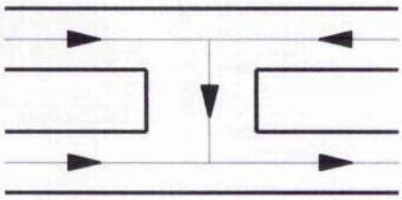

Figure 5-29: Schematic of bank 2 flow

When an inlet valve in bank 1 cylinder opens (Fig. 5-24), air is delivered from upstream of the connection pipe and through it. Air entering through the connection pipe is derived from upstream and downstream of bank 2 (illustrated in Fig. 5-25). Figure 5-26 shows the flow field after the inlet valve closes, but before a bank 2-cylinder inlet valve opens. Air passes above and below the connection pipe, but not through it. Figure 5-28 shows the flow field as air passes to a bank 2 cylinder. Air is derived from upstream, as well as through, the connection pipe. However, air passing through the connection pipe is derived from upstream and downstream directions simultaneously. Thereby, a significant flow interaction occurs inside the connection pipe (vide Fig. 5-29).

Air flowing in the charge air pipe must react more quickly to the opening and closing of inlet valves at increasing engine speeds. Whereas to the two separate flow situations observed in the 2000-rpm case, here a single flow of air passes through the connection pipe (Figs. 5-28, 5-29). Thereby producing a more defined pressure curve, refer Fig. 5-23. A pressure difference of 0.3 bar is observed in bank 2 at 3000 rpm, whereas 0.075 bar at 2000 rpm, refer Figs. 5-23 and 5-13 respectively.

Case 3: 4000 rpm

Figure 5-30 shows the predicted pressure varying with crank angle in bank 1 at 4000 rpm. Pressure waves in evidence are reproduced by the hybrid prediction. Higher frequency

oscillations overlay low-frequency waves, as is confirmed by the experimental measurements. A shoulder is generated in the measured pressure profile when a bank 1 inlet valve opens at 370°CA. This phenomenon is reproduced by the hybrid computational. Though the amplitude in bank 1 calculated at 4000 rpm is higher than that at 3000 rpm, the predicted amplitude does not match the experimental measurement.

Comparing the figures below with those found at an engine speed of 3000 rpm, a phase shift is observed once more. The increase of engine speed from 3000 to 4000 rpm caused the pressure waves to shift through 40 to 45°CA.

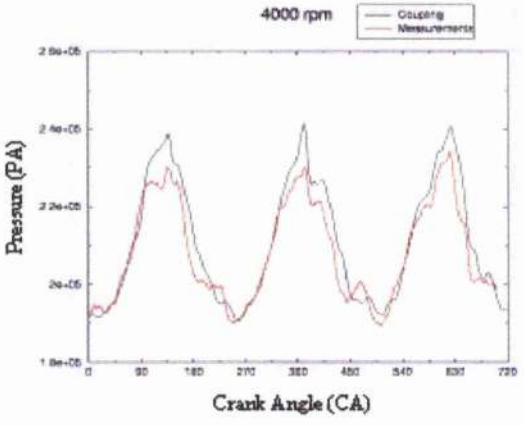

Figure 5-30: Bank 1 at 4000 rpm

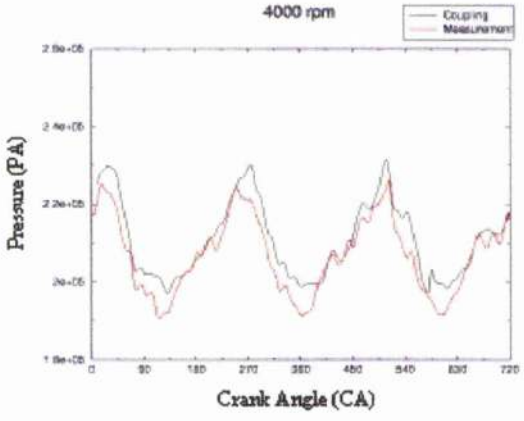

Figure 5-31: Bank 2 at 4000 rpm

Pressure curves in bank 2 illustrated in Fig. 5-31 correspond to an engine speed of 4000 rpm. High frequency oscillations are evident, superimposed on pressure waves generated at engine frequency. These higher frequency oscillations are attributable to unsteady and varying flows in the connection pipe. At this higher engine speed, the airflow is less able to respond to the engine, breathing air, and the rounded pressure waveforms seen at lower speeds are no longer present.

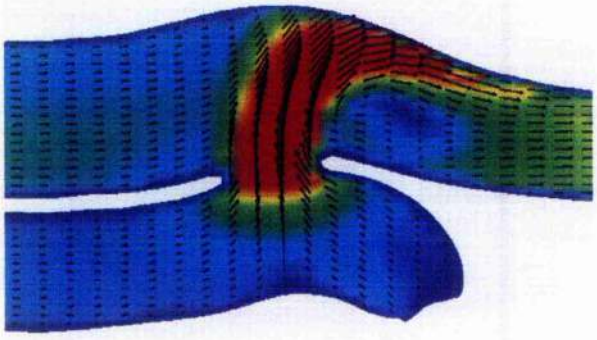

Figure 5-32: Flow to Bank 1 at 4000 rpm

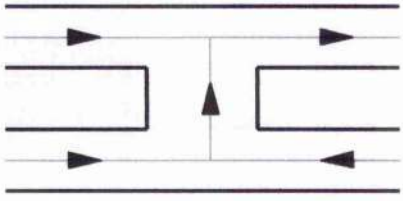

Figure 5-33: Schematic of bank 1 flow

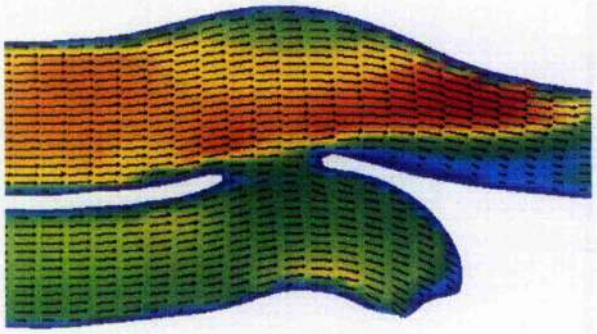

Figure 5-34: No flow through connection pipe

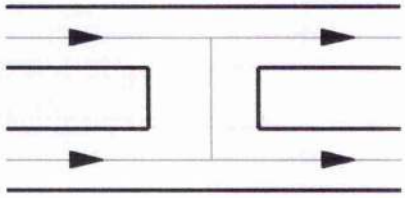

Figure 5-35: Schematic of no flow through connection pipe

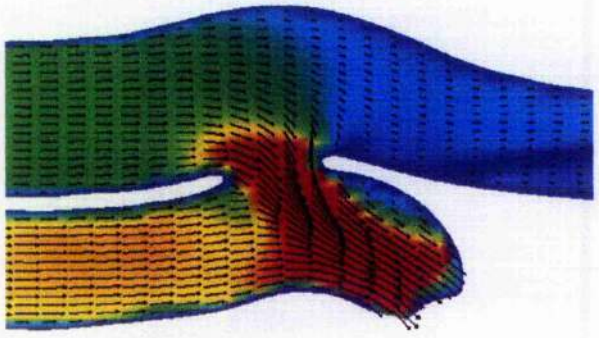

Figure 5-36: Bank 2 flow at 4000 rpm

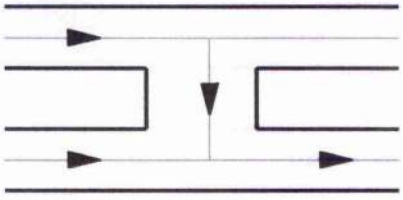

Figure 5-37: Schematic of bank 2 flow

Flow field results for an engine speed of 4000 rpm are presented in Figs. 5-32 to 5-37. Figure 5-32 shows the calculated field at the instant at which an inlet valve opens in bank 1. Air enters from upstream and via the connection pipe. At this high engine speed, flow in the connection pipe to bank 1 disturbs the upstream airflow. The effect is equivalent to a reduction of the effective cross-sectional area of the pipe leading to bank 1. The calculated flow field at the instant that a bank 1 inlet valve closes is shown in Fig. 5-34. Air passes upstream and downstream of the connection pipe, but not through it. Figure 5-36 illustrates the calculated flow field when an inlet valve is open in a bank 2 cylinder. Air enters the cylinder from upstream of the connection pipe and via this pipe. Air that passes through the connection pipe is derived from the upstream, but not the downstream.

5.4.2.3 Modified Charge Air Pipe

Benefiting from knowledge of the propagation of pressure waves in the original pipe system, the connection pipe was moved with the aim of increasing airflow to the engine at high speeds. Figure 5-38 defines the modified geometry.

Figure 5-38: Altered geometry of the charge air pipe

Results

The projection plane defined in Fig. 5-9 is retained. Schematics that simplify the representation of flow phenomena around the connection pipe are provided, as before. The results shown are for an engine speed of 2000 rpm. The volumetric efficiency of the original air charge pipe peaked near to 2000 rpm and the hybrid model is more stable and computationally swift at low speeds.

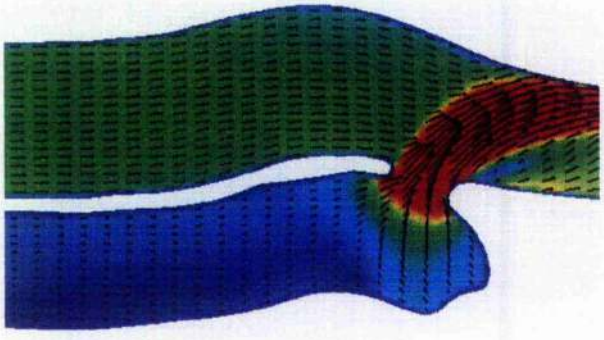

Figure 5-39: Bank 1 flow

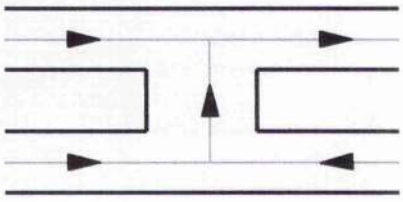

Figure 5-40: Schematic of bank 1 flow

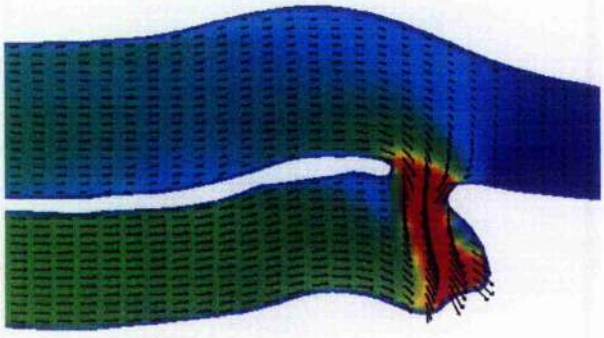

Figure 5-41: Bank 2 flow

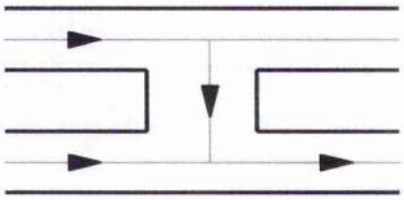

Figure 5-42: Schematic of bank 2 flow

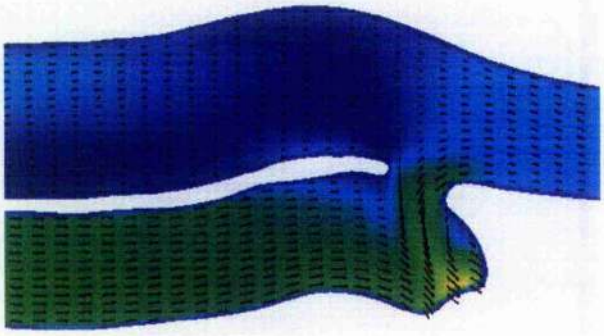

Figure 5-43: Weaker bank 2 flow

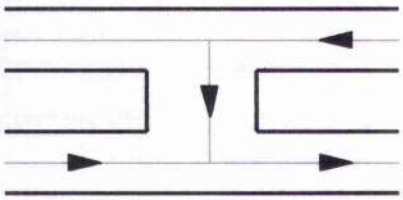

Figure 5-44: Schematic of weaker flow

Figures 5-39 through 5-44 present the sequence of events predicted for the altered geometry. When an inlet valve of a cylinder in bank 1 opens, air flows through the connection pipe from bank 2, Fig. 5-39. High velocity air passing through the connection mixes with air drawn through the inlet pipe and the mixed flow enters bank 1. Figures 5-41 and 5-42 represent the airflow when an inlet valve of a cylinder in bank 2 opens. As the in the original geometry (Fig. 5-8), air initially flows from upstream of the connection pipe before entering bank 2 (Fig. 5-16). Thereafter, air flows through the connection pipe from downstream, i.e. from bank 1, but the shift of the connection pipe reduces the magnitude this flow. However, less air passes from the downstream (bank 1) when compared to that flowing in the original geometry,

Figures 5-45 & 5-46 compare pressure results predicted between the modified and original geometries at locations corresponding to pressure transducers 1 and 2 in Fig. 5-5.

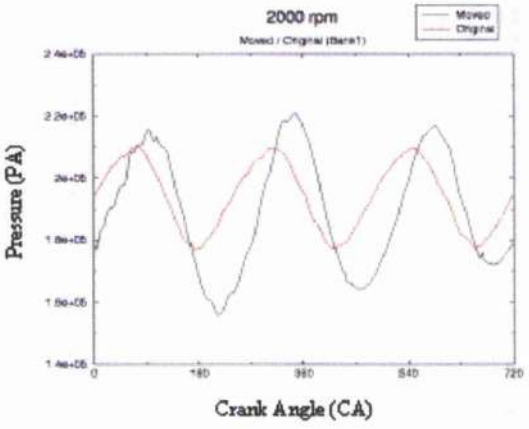

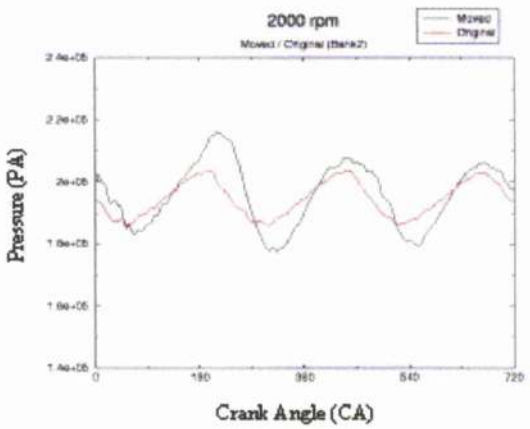

Figure 5-45: Altered v Original: Bank 1 at 2000 rpm *Figure 5-46: Altered v Original: Bank 2 at 2000 rpm*

Pressure amplitudes in the modified geometry model are notable raised: the difference in pressure of the maximum and minimum peaks on the profile is 0.6 b in the modified pipe and 0.3 b in the original geometry. Furthermore, the pressure profiles are temporally displaced one from the other; the phase shift calculated at bank 1 (being furthest removed from the connection pipe) is marked. Thereby, the modification significantly reduces the volumetric efficiency.

5.5 Engine Simulations: Conclusions

When experimentally determined loss coefficients are applied, the 1D numerical technique reproduces the performance characteristics of the engine closely. The method is economical: a 1D calculation of a complete engine may take a number of hours, whereas a multi-dimensional computation might occupy days or even weeks. However, a considerable experimental effort is required to establish the loss coefficients.

Flow effects in the region close to the connection pipe cannot be analysed in detail, for the 1D model represents the flow with a singe computational node. It is impossible to envision the flow phenomena inside the charge air pipe. None the less, the close agreement of experimental and predicted results validates the use of this 1D representation of the engine for the purposes of instantiating the unsteady, hybrid model, which is developed herein.

Flow fields predicted by the hybrid methodology compared well with experimental results. The hybrid scheme successfully combines a 1D model that calculates transport times between geometric discontinuities accurately with a 3D model that manages complexity and estimates losses. The hybrid model of the charge air pipe was established quickly and without the need for experimentally determined loss coefficients. The 3D mesh must be constructed with care and be adapted to resolve the flow geometry elegantly. Transient flow fields being unpredictable, it is difficult, *ab initio,* to create an optimal mesh.

Figures 5-14, 5-24 and 5-32 show air flowing through the connection pipe into cylinder bank 1 at the calculated engine speeds. In all three cases, the flow enters from upstream of the connection pipe and from bank 2.

In contrast, air enters cylinder bank 2 from the volume before the connection pipe, and from bank 1, i.e. from downstream of the connection pipe, at 2000 and 3000 rpm. The volumetric efficiency (Fig. 5-4) was highest at 2000 rpm, consistently with the supply of air in successive time intervals, first from the inlet region and subsequently from cylinder bank 1. The volume of air entering via the connection pipe from downstream decreases as the engine speed increases and the volumetric efficiency falls. This effect reaches an extreme at 4000 rpm, when bank 2 no longer receives air via bank 1.

The hybrid model reacted sensitively to high engine speeds; it crashed on one occasion when computing the 4000 rpm case. A small area near to the coupling interface developed extreme velocities just prior to the termination. This caused the velocity vector to flip at the 1D/3D interface within the space of a single time step. Calculated the transient on shorter time interval by reducing the default time step circumvented this difficulty.

The volumetric efficiency of the engine is greatly affected by flows in the connecting pipe and, therefore, upon its positioning in the air charge pipe. The hybrid scheme has demonstrated capacities to represent this sensitivity and explain it and to serve as a powerful rapid prototyping tool. Bench tests cannot resolve the complexity of flows near the connecting pipe and lack the finesse necessary to represent or interpret speed dependent loss mechanisms that prevail in the charge air pipe.

6 CONCLUDING REMARKS

The research has created a method that reduces the computational burden of calculating unsteady flows within internal combustion engines. The hybrid method evolved provides for the analysis of complex engine components into regions that are describable, appropriately, by either three-dimensional or one-dimensional schemes. The method connects these contiguous regions via computational interfaces that ensure the compatibility of the 3D and 1D descriptions that coincide at them.

The work presented began with the purpose of improving the accuracy of boundary conditions employed in pipe systems and reduce the dependency on measured data.

The primary elements of the hybrid are:

- A one-dimensional model that represents the global system as a series of interconnecting pipes for the purposes of a global solution. This model is rendered numerically in a finite difference scheme and solved by an explicit method, the latter moderated by a stability criterion that prescribes a maximum time interval. To close the model of the global system, experimentally determined losses are required at discontinuities in the system.
- Three-dimensional models of regions of the subject component that sustain complex flows and which, being embedded in the global model, create the hybrid representation. These models are rendered numerically in a discrete volume scheme and are solved by an implicit method. Turbulence models are used to predict losses in complex flows, these models circumvent the dependence on experimental determinations of losses.
- Interface constructs that ensure the integrity of a hybrid model by controlling the exchange of information between the three-dimensional and one- dimensional regions on which it is constructed and manage the dissimilar computational representations that stand on either side of the interface. Interfaces must be computationally transparent if they are not to generate spurious pressure transients. The interface methodology comprises:
    - A data transfer scheme that upholds the conservation laws at interfaces of contiguous 1D and 3D regions and establishes transient boundary conditions that permit the solution to continue. An averaging technique sums the multiple data points presented by a 3D region and instantiates the single data point representing a 1D region. A scheme that infers a velocity distribution, consistently with a single 1D data point, and impresses it at the entry to a 3D region significantly improves predictions of losses incurred within the region.

- o A coupling method to evaluate data transferred at the interface. Two methods were discussed; a simple boundary face method, which would prove difficult to synchronise temporally, and a recommended, if more complex method, which overlaps the 1D and 3D domains at the interface.
- o Synchronisation of the differing implicit and explicit temporal discretisation schemes used by the 3D and 1D numerical methodologies relies on the overlap strategy to rectify the inherent discrepancy of one time interval.

The hybrid scheme was validated by its application to the unsteady flow in the charge air pipe of an Audi 2.0 litre turbo diesel engine. Comprehensive bench test data was available. The hybrid model predicted the variation of the engine's volumetric efficiency with speed and reproduced transient pressure profiles at sites where pressure transducers recorded experimental data. Furthermore, using 3D CFD post-processing techniques a more detailed understanding of the flow field within the charge air pipe was achieved.

The following chart shows the hybrid methodology incorporated in Volkswagen's process chain.

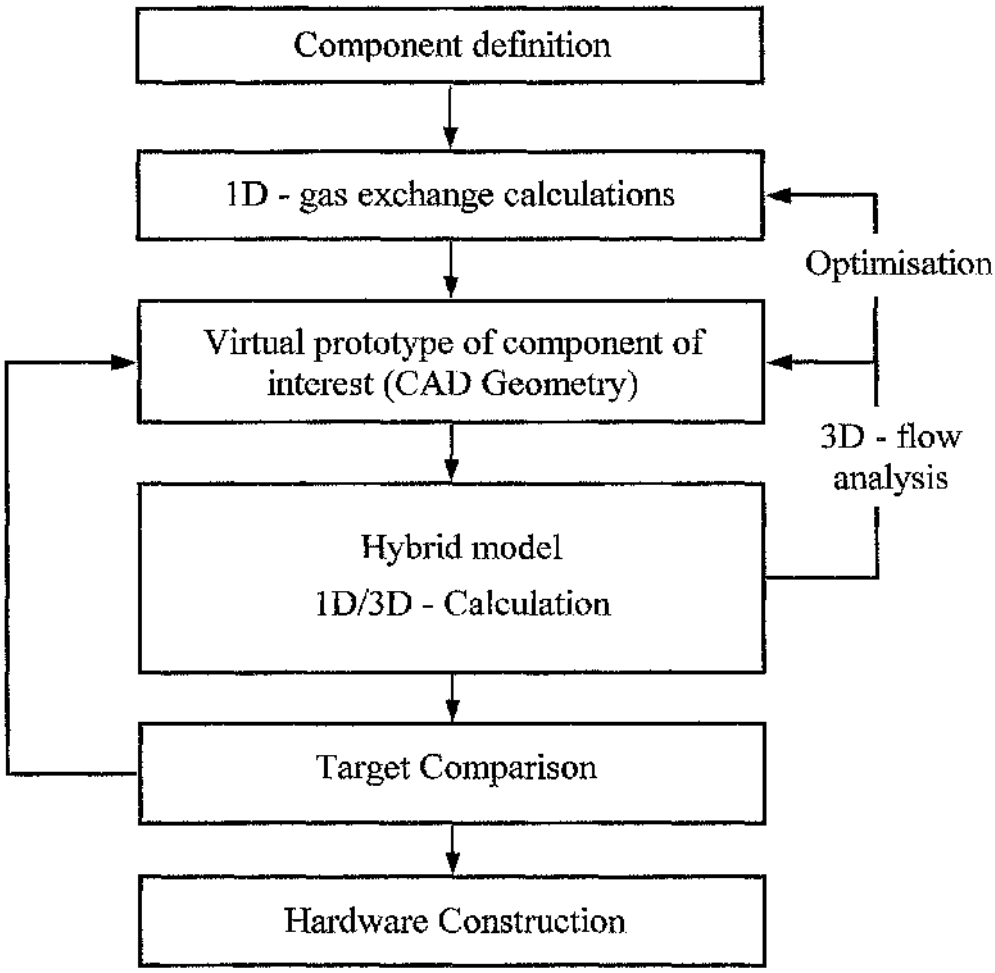

Figure 6-1: Hybrid calculations within the process chain

Design starts with a one-dimensional analysis of a simple model that interprets the component definition. Loss coefficients required are estimated from parametric studies or else inferred from similar practice. The analysis into regions where three-dimensional influences dominate depends upon the construction of a virtual prototype captured by a suitable CAD system. Thence, the hybrid is constructed so that the consonance of flows near interfaces of 1D and 3D regions may be affirmed. Insights revealed by the hybrid model inform design judgements and thereby the solution converges on the specified performance. The part is manufactured for the first time when the design is validated by predictions of its performance.

6.1 Further work

The research is not exhausted. Investigations of exhaust systems and the re-circulation of exhaust gases into the inlet system would be advanced by an application of the hybrid system that accounted for the chemical species present in the flow. A first step might incorporate equations of state that represented equilibrium states of mixtures of gases. The computational burden of solving rate equations, e.g. in a catalytic converter, would constrain such calculations to 1D regions. Furthermore, the inclusion of an exhaust system would affect the time step size and expand the computational burden.

Computation in multiple processors of flows in three-dimensional domains, would greatly speed the calculation. Individual processor, working simultaneously, could compute solutions in contiguous sections of the 3D component. However, interfaces between one and three-dimensional models would be made more complex. A single processor might be assigned to the computation of all interfaces with advantage won when averaging flows and transferring the data between regions of the hybrid model.

The application of genetic algorithms would reduce reliance on hardware prototypes. The computational power required is currently so great as to leave this option inaccessible to industrial engineers.

7 REFERENCES

1. Bianchi, G. M., Cantore, G., Fontanesi S.: "Turbulence Modelling in CFD Simulation of ICE Intake Flows: The Discharge Coefficient Prediction", SAE 2002-01-1118.
2. Smirnov, A., Yavuz, I., Celik, I.: "Diesel combustion and LES of in-cylinder turbulence for IC-engines", ASME paper 99-ICE-247.
3. Siebert, W., Lanfrit, M., Hupertz, B., Krueger, L.: "A Best Practice for High Resolution Aerodynamic simulation around a Production Car Shape", 4th MIRA International Vehicle Dynamics Conference, Oct. 2002
4. Benson, R. S.: "The Thermodynamics and Gas Dynamics of Internal Combustion Engine", Vol. 1, Clarendon Press, Oxford, 1982.
5. Bingham, J.K; Blair, G.P.: "An improved branched pipe model for multi-cylinder automotive engine calculations", SAE 854998
6. Blair, G. P., Mackey, D. O., Ashe, M. C., Chatfield, G. F.: "On improving the accuracy of the simulation of reciprocating engines", 2000-04-0364.
7. Gosman, A. D.: "Multidimensional modelling of cold flows and turbulence in reciprocating engines", SAE 850344.
8. Bolton, B.; Takenaka, Y.; Nakajima, H.; Aayagi, Y.; Yoko, I.: "Analysis of intake manifold in an incline 6 cylinder DI engine", SAE 938146.
9. Kuo, Tang-Wei; Chang, S.: "Three-dimensional steady flow computations in manifold-type junctions and a comparison with experiment", SAE 932511.
10. Wulf, A., Steberl, R., Akdag, V.: "Efficient Integration of CFD into Product Design" Presented 1999 at the von Karman Institute for Fluid Dynamics, Belgium.
11. Mazy, P., Hager J., Reitbauer R.: "Integration of 1D and 3D simulation models for typical Applications in Automotive Thermal Management", VDI report Nr 1559, 2000.
12. Winterbone, D. E., Pearson, R. J.: "Design techniques for engine manifolds – Wave action methods for IC Engines", Professional Engineering Publications, London, 1999.
13. Launder, B. E., Spalding, D. B.: "The Numerical Computation of Turbulent Flow", Computer Methods in Applied Mechanics and Engineering Vol.3 1974.
14. Shaw, C. T., Lee, D. L., Richardson, S. H., Pierson, S.: "Modelling the Effect of Plenum-Runner Interface Geometry on the Flow Through an Inlet System", SAE 2000-01-0569.

15. Strauss, T. S.: "Simulation der Verbrennung und NOx -Bildung in einem direkteinspritcnden Dieselmotor mit externer Abgasrückfuhrung", Dissertation, RWTH Aachen, 1999.

16. Heywood, J. B.: "Internal Combustion Engine Fundamentals", McGraw-Hill, 1988.

17. Schindler, P.: "Berechnungsmodelle für instationäre Strömungsvorgänge durch Mehrfachverzweigungen im Rohrleitungssystem von Verbrennungsmotoren", Dissertation, Ruhr-Universität Bochum, 1990.

18. Bird, R. B., Stewart, E. W., Lightfoot, E. N.: "Transport Phenomena", John Wiley and sons, 1960.

19. Seifert, H: "Instationäre Strömungsvorgänge in Rohrleitungen an Verbrennungskraftmaschinen", Springer, 1962.

20. Seifert, H.: "Erfahrungen mit einem mathematischen Modell zur Simulation von Arbeitsverfahren in Verbrennungsmotoren", MTZ 39, 1978.

21. Stromberg, H. J.: "Ein Programmsystem zur Berechnung von Verbrennungsmotor-Kreisprozessen mit Berücksichtigung der instationäre Strömungsvorgänge in den realen Rohrleitungssystem von Mehrzylider-Verbrennungsmotoren", Diss. Ruhr-Universität Bochum, 1977.

22. Mayr, B.: "Beitrag zur Berechnung des Ladungswechsels an Verbrennungskraftmaschinen mit besonderer Berücksichtigung der instationären Strömung in Rohrleitung", Diss. T.U. Berlin, 1969.

23. Seifert, H.: "A mathematical model for simulation of processes in an internal combustion engine", Pergamon Press, 1979.

24. Anderson, D. A., Tannehill, J. C., Pletcher, R. H.: "Computational Fluid and Mechanical Heat Transfer", Hemisphere, 1984.

25. Courant, R., Friedrichs K. O., Lewy H.: "Uber die Differenzengleichungen der Mathematischen Physik", Math. Ann. Vol. 100 , 1928.

26. Fletcher, C. A. J., "Computational Techniques for Fluid Dynamics", 2nd Edition, Spinger Verlag, 1997.

27. STAR-CD Manual, Version 3.05, 1998.

28. STAR-CD Methodology, Version 3.05, 1998.

29. Rodi, W.: "Turbulence models and their application in Hydraulics – A state of the art review", June 1980.

30. Wilcox, D. C.: "Turbulent modelling for CFD", DCW Industries, Inc., California, 1998.

31. El Tahry, S. H.: "k-e equation for compressible reciprocating engine flows", AIAA J., 1983.

32. Yakhot, V., Orszag, S. A.: "Renormalization group analysis of turbulence – I: Basic Theory", J. Scientific Computing, 1986.

33. Chen, Y. S., Kim, S. W.: "Computation of turbulent flows using an extended k-e turbulence closure model", NASA CR-179204, 1987.

34. Versteeg, H. K., Malalasekera, W.: "An introduction to Computational Fluid Dynamics", Longman Scientific & Technical, 1995.

35. Gosman, A. D., Pun, W. M., Runchal, A. K., Spalding, D. B., Wolfstein, M.: "Heat and mass Transfer in Recirculating Flows", Academic Press, London, 1969.

36. Peric, M: "A Finite Volume Method for the Prediction of Fluid Flow in Complex Ducts", Thesis, Imperial college, 1985.

37. Hirsch, C.: "Numerical Computation of Internal and External Flows – Vol. II: Computational Methods for Inviscid and Viscous Flows", John Wiley and Sons, New York, 1960.

38. Peric, M., Ferziger, J. H.: "Computational Methods for Fluid Dynamics", Springer, 1996.

39. Laney, C. B.: "Computational Gas Dynamics", Cambridge University Press, 1998.

40. Patankar, S. V.: "Numerical Heat Transfer and Fluid Flow", McGraw-Hill Book Company, New York, 1980.

41. Traupel, W.: "Thermische Strömungsmaschinen Band 1", Springer, Berlin, 1966

42. Schlichting, H.: "Boundary layer theory", McGraw-Hill, New York, 1968.

43. "10 Jahre TDI-Motor von Audi", Motortechnische Zeitschrift Sonderausgabe, 1999.

44. Smith, L. A., Fickenscher, T., Osborne, R. P.: "Engine Breathing – Steady Speed Volumetric Efficiency and its Validity Under Transient Engine Operation", SAE 1999-01-0212.

45. Audi internal report

46. T. Asanuma, T.Obokata: "Gas Velocity Measurements of a Motored and Firing Engine by Laser Anemometry", SAE paper 790096.

47. "The ERCOFTAC Best Practice Guidelines for Industrial Computational Fluid Dynamics", Version 1, ERCOFTAC, 2000.

48. Anderson, J.D.: "Modern compressible flow, with historical perspective", McGraw-Hill, New York, 1990.

49. Anderson, J. D. Jr.: "Computational Fluid Dynamics, The basics with applications", McGraw-Hill, 1995.

50. Blair, G .P., Lau, H. B., Cartwright, A., Raghunathan, B. D., Mackey, D. O.: "Coefficients of Discharge at the Apertures of Engines", Design and Emissions of small Two- and Four Cylinder Engines, pp. 71-85, (SP-1112), 1995.

APPENDICES

A: Need for Two Way Coupling Illustrated

The schematic below shows two models having a volume a connected to a number of pipes (arrows indicate direction of flow – inlet (green), exit (blue)).

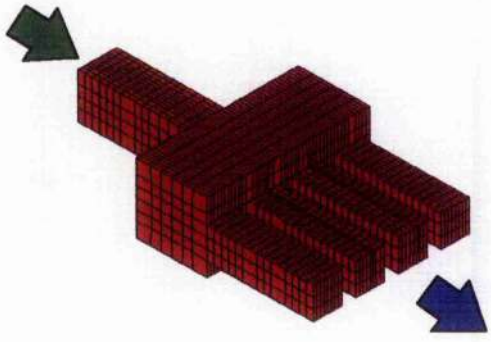

Figure A-1: Top Flow model

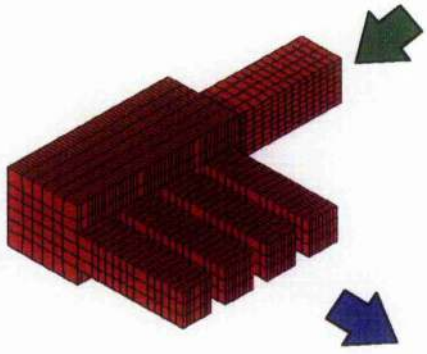

Figure A-2: Side Flow model

These three-dimensional models illustrate different flow fields consequent upon marginal changes in geometry. Comparisons are made with a 1D analysis of the same system.

A.1 Three Dimensional Model Results

- Top flow model: flow entering from the top of the volume

The 3D model contains circa 20000 fluid cells. A pressure difference of 0,2 b is applied to the entire system. Figure A-1 plots the results obtained.

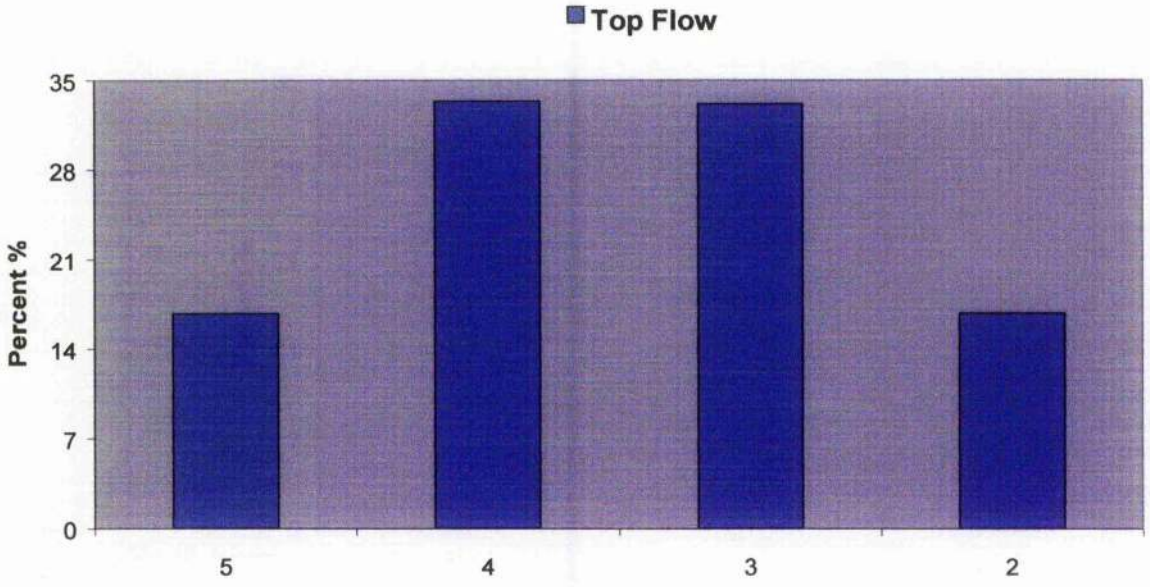

Figure A-3: Mass flow results for the Top Flow model

The graph shows the relation between the inlet (100%) and exit mass flow at each pipe leaving the volume. The x-axis of Fig. A-3 represents the outlet pipes.

Clearly the influence of the multidimensional model produces non-uniform pressure values at the exiting pipes in the two-way coupling calculations. The model being symmetrical, the mass flow entering the inside pipes (4, 3) should be the same and similarly for the two outside pipes (5, 2). The graph shows this to be true.

- Test case 2 flow entering from the side of the volume

The model set-up is identical to that of case 1.

The multidimensional model used in this analysis is show in Fig.A-2. Results of a 3D calculation are given in Figure A- 4.

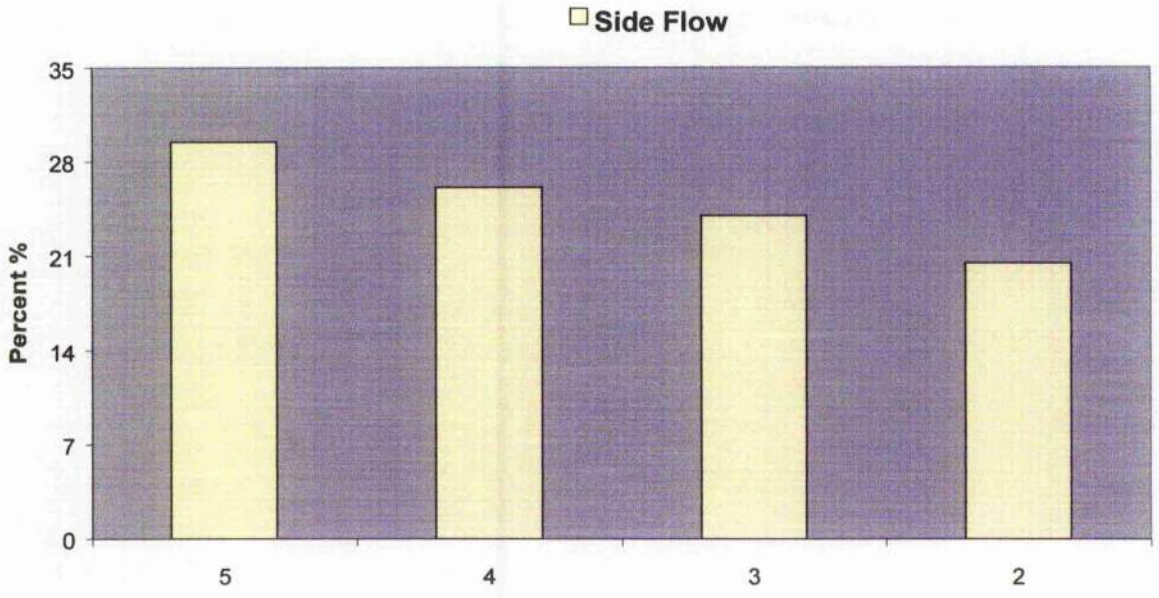

Figure A-1: Mass flow results for the Side Flow model

The relationship of the inlet and exit mass flows is shown against the pipe number in the above, Fig A-4. The exit pipe furthest from the inlet pipe contains the highest value of mass flow. The mass flow decreases in each consecutive pipe, with the pipe nearest the inlet allowing the smallest mass flow.

A.2 One Dimensional Model

The one-dimensional fluid numerical tool employs the schematic of Figure A- 5.

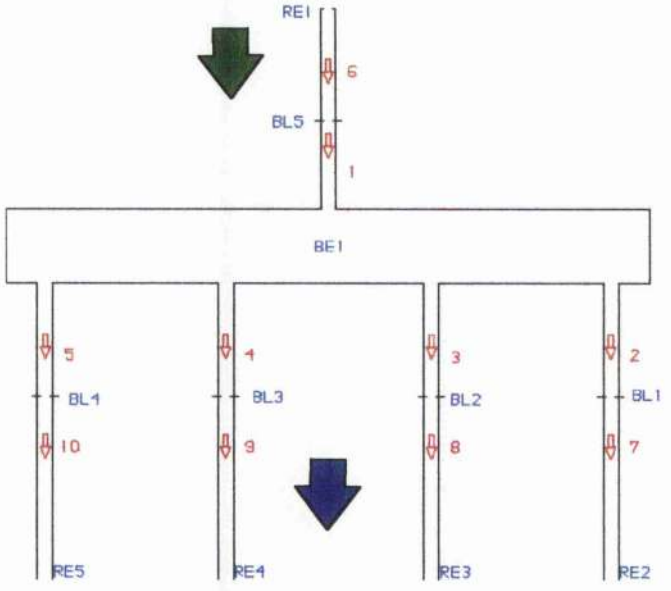

Figure A-2: 1D model of the inlet manifold

The positioning of the orifices (BL1 – 5) coincides with the locations of coupling interfaces (i.e. no losses occur over the orifices). Each orifice represents a boundary region to a 3D model.

The 1D model does not account for the different inlet flows to the main volume. A loss coefficient must be applied at both ends of each pipe in the 1D system to represent losses associated with each pipe connection to the main volume. So that an accurate numerical analysis of each model can be made the loss coefficients should not be the same in each model. When the loss coefficients are identical for each connection, a 1D analysis should allocate 25% of the inlet total flow to each pipe. The numerical analysis applies the same loss coefficients to each connection. The results compare a 1D numerical analysis of the system with a two-way coupling.

The graphs of Fig A-6 provide the comparison.

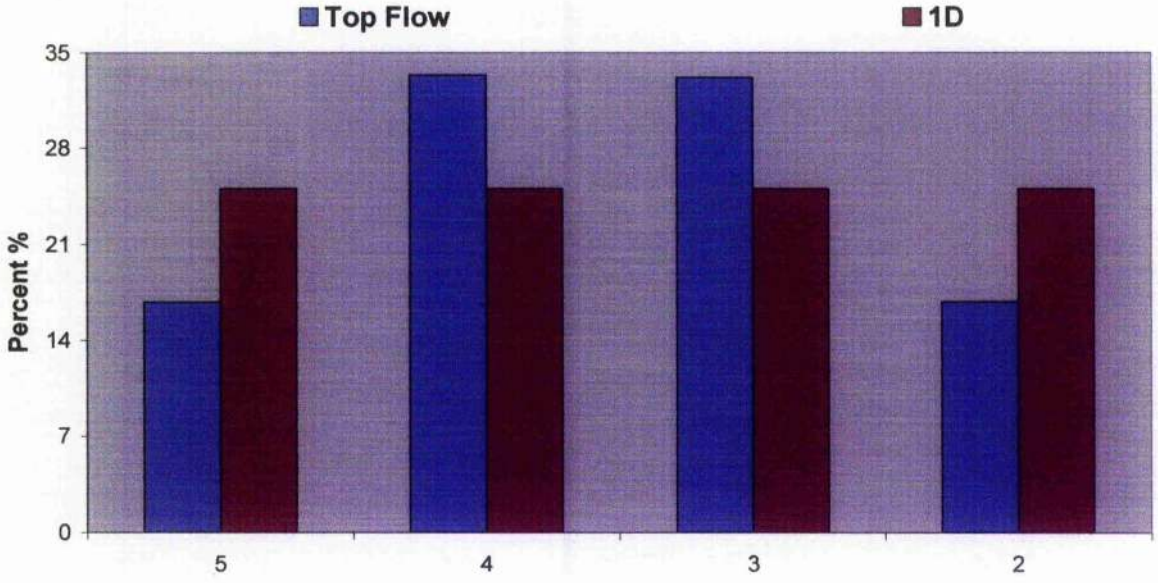

Figure A-3: Comparison between 1D and hybrid model (Top Flow)

The 1D results show equal contributions each exiting pipe.

This result emphasises the importance of specifying loss coefficients accurately in 1D models. The results found from the two-way coupling can now be used to calibrate the 1D model and provide suitable loss coefficients for each pipe connection.

Comparison of the side flow example with 1D results produces the results plotted in Fig. A-7.

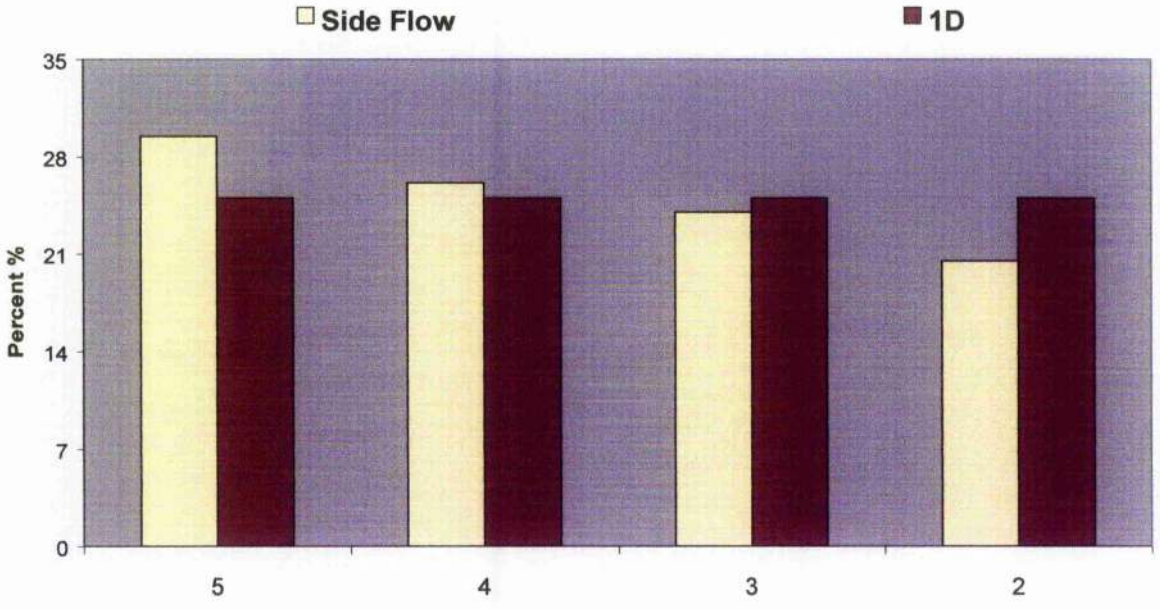

Figure A-4: Comparison between 1D and hybrid model (Side Flow)

As shown previously, the 1D result predicts identical outputs from each exit pipe. Therefore, if a numerical analysis of the system is to be conducted, the loss coefficients cannot be the same as those applied to the previous test case.

These results show that 3D results do not coincide with 1D predictions unless the 1D loss coefficients are correctly applied. 1D model loss coefficients are best calibrated with measurements taken from bench tests. In the absence of test results, either estimated values must be used or a 3D analysis must be substituted. The 3D and 1D models must be reset so that only one exit pipe is open. This procedure must then be repeated for successive pipes.

A.3 Conclusion

The aim of the above was to illustrate the disadvantages of the parabolic boundary definition, imposing time varying boundary conditions onto a 3D flow domain. With this method time varying boundary conditions are found from a previously calculated 1D numerical analysis of the system, the information found from this analysis are then applied to the 3D flow domain. In order to illustrate the limitations of the 1D method the results of the 1D calculations were compared with 3D calculations. From the graphs presented the differences between the 1D analysis and the 3D analysis can be seen. Furthermore, the flow information found in the 3D calculations cannot be transported to the 1D model, thereby improving the 1D calculations. This one-way nature of the current method leads to inaccuracies in the overall results.

B: Averaging the Three Dimensional Flow Distribution

B.1 Introduction

Close management of the coupling interface is critical to accurate transfer of flow information from the 3D to 1D flow domains. The averaging method is at issue.

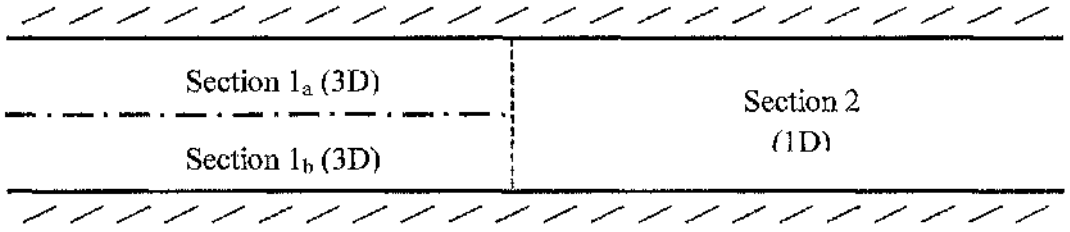

Figure B-1: Schematic to illustrate averaging technique

Figure B-1 shows a pipe of constant diameter split into two sections, which are modelled in 3D and 1D respectively. The 3D domain is further divided into two sections, 1_a and 1_b. The aim of the averaging technique is to transfer flow information from section 1 to section 2 with a minimum loss of accuracy.

Conservation of mass, momentum and energy are ensured [23] by the following:

Mass

$$\left[\sum_i^n\left(\frac{p_i w_i A_i}{RT_i}\right)\right]_1 = \left[\frac{\overline{p}\cdot\overline{w}A}{R\overline{T}}\right]_2. \qquad \textit{Eq. B.1}$$

Momentum

$$\left[\sum_i^n\left(\dot{m}_i w_i + p_i A_i\right)\right]_1 = \left[\dot{m}_{1D}\overline{w} + \overline{p}A\right]_2. \qquad \textit{Eq. B.2}$$

Total Energy

$$\left[\sum_i^n \dot{m}_i\left(c_p T_i + \frac{1}{2}w_i^2\right)\right]_1 = \left[\dot{m}_{1D}\left(c_p\overline{T} + \frac{1}{2}\overline{w}^2\right)\right]_2. \qquad \textit{Eq. B.3}$$

Entropy

$$\left[\frac{1}{\dot{m}_{total}}\sum_i^n s_i\dot{m}_i\right]_{3D} = \left[\frac{1}{\dot{m}_{1D}}s_{1D}\dot{m}_{1D}\right]_{1D} \qquad \textit{Eq. B.4}$$

Traupel [21] has described averaging methods, including:

1 the use of the mass, momentum and energy equations,

2 adopting a constant pressure, along with the mass and energy equations, and finally

3 utilising the mass, energy and entropy equations.

These averaging techniques are evaluated herein.

B.2 Model Set up

Regions 1_a and 1_b (Fig.B-1) have identical mass flows and the same cross-sectional areas. Though the pressures are equal, the gas temperature and fluid velocity differ. This input data permits the conservation laws to be evaluated in each section of the pipe:

Section	Mass Flow (kg/s)	Total Energy (H0)	Momentum (N)	Entropy (J/kg K)
1a	0.13678	41917.13	131.488	6817.37
1b	0.13678	49036.51	133.768	6972.27
2	0.27356	90953.83	265.255	6894.82

The constants are: ratio of specific heard $\kappa = 1.4$, characteristic constant $R = 287.1$ and $c_p = 1004.8$.

The values for section 2 in the table above are calculated by summing each corresponding quantity. The data given in the table are used in the averaging procedures for each method given below.

B.3 Averaging Methods

B 3.1 Mass, Momentum and Energy Equations

With these equations, the velocity can be expressed in a quadratic equation. With the average velocity determined the values of pressure and temperature follow.

The results can be summarised in the following table

Section	Mass Flow (kg/s)	Total Energy (H0)	Momentum (N)	Entropy (J/kg K)
1a	0.13678	41917.13	131.488	6817.37
1b	0.13678	49036.51	133.768	6972.27

Averaged	0.27356	90908.97	267.81	6894.31

As expected, the values of continuity, momentum and energy match those found in the initial table. However, the value of entropy differs from that found previously, a slight increase is observed.

Therefore, the application of this averaging method must assume that the entropy increases. The extent of this entropy increase can be seen when an averaging method is used which conserves the entropy.

B 3.2 Continuity, Energy and Entropy Equations

The equations of continuity, energy and entropy are used to find the average values. The results are shown in the following table.

Section	Mass Flow (kg/s)	Total Energy (H0)	Momentum (N)	Entropy (J/kg K)
1a	0.13678	41917.13	131.488	6817.37
1b	0.13678	49036.51	133.768	6972.27
Averaged	0.27356	90908.97	270.347	6891.28

An iterative approach is required to solve these equations. However, after the values of velocity, pressure and temperature are found the conservation laws are calculated. Continuity, energy and entropy laws match those found initially, however the momentum law is not upheld.

The results given above show a constant value of entropy at the coupling interface. The difference between this value and the entropy found in the previous method can be found, and is relative small (~0.2%).

B 3.3 Continuity, Energy and Constant Pressure

Assuming constant pressure throughout, and using the mass and energy conservation laws, the velocity is determined from a quadratic equation. As before, with a known mean velocity the mean pressure and temperature can be found. The following table gives the results.

Section	Mass Flow (kg/s)	Total Energy (H0)	Momentum (N)	Entropy (J/kg K)
1a	0.13678	41917.13	131.488	6817.37
1b	0.13678	49036.51	133.768	6972.27
Averaged	0.27356	90908.97	267.83	6894.31

Since the conservation laws of continuity and energy are used, it is expected that the values are identical to those found initially. However, the values of both momentum and entropy fail to match those shown previously.

B 4 Conclusions

In order to transfer flow conditions from a multi-dimensional flow domain to a 1D flow domain an averaging technique must be adopted. The above discussion illustrated three possible methods that can be used to achieve this goal. It was shown that independent of the equations, a small error is produced. These results are discussed fully in [21].

C: Interface Placement

The need for careful consideration when locating the position of coupling interfaces is illustrated. A pipe system similar to the inlet manifold of a four-cylinder internal combustion engine is modelled.

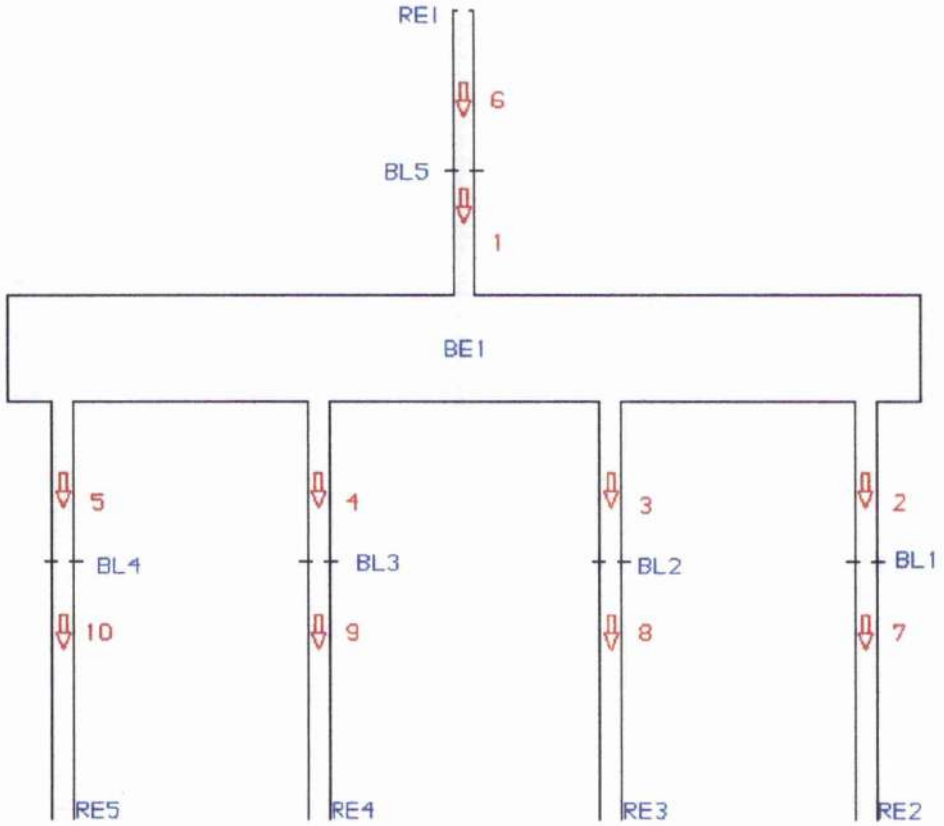

Figure C-1: Schematic of boundary placement model

The 3D part of the hybrid model is enclosed within dashed lines.

Variations to this 3D model were introduced by varying the lengths of the ports. Figures C-2 through C-7 give the details. The pipe system remains unchanged: reductions in the length of the 3D section are compensated by increases in the lengths of 1D pipe sections. Initial conditions and boundary conditions placed in the entire system were held constant.

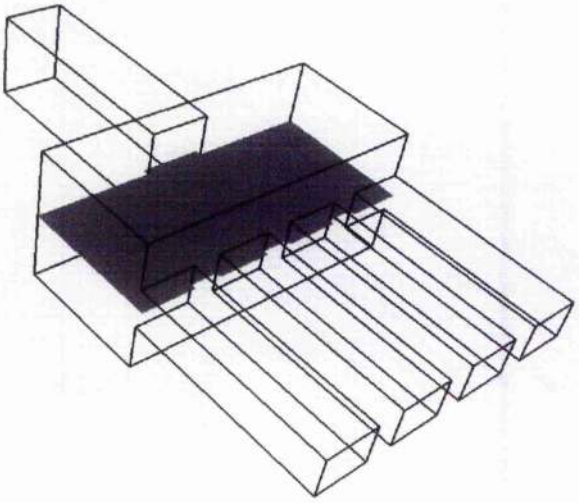

Figure C 2: Long pipe model

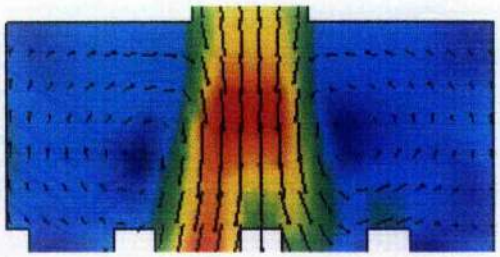

Figure C-3: Long pipe results

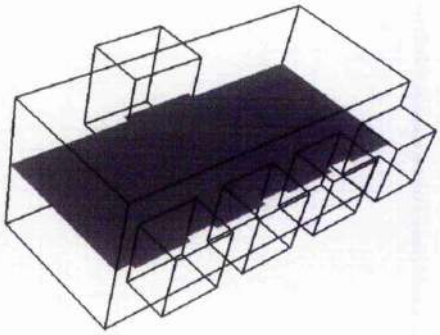

Figure C-4: Short pipe model

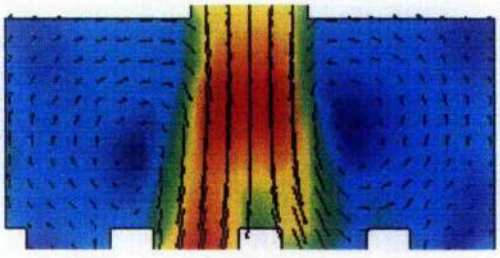

Figure C-5: Short pipe results

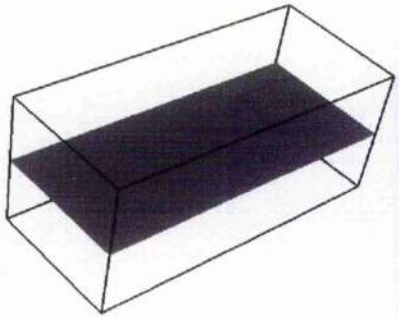

Figure C-6: No Pipe model

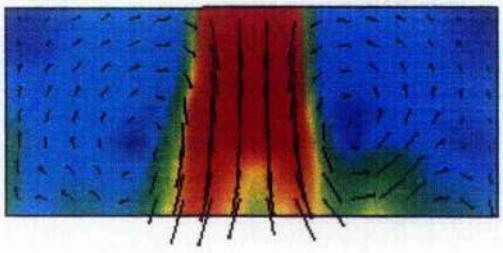

Figure C-7: No pipe results

Figures C-3, C-5 and C-7 depict the flow field inside the main volume of the manifold for successive variations of the model. The results are compared at the same time step. A section plane taken through the centre of each 3D model is drawn in the figures. The arrows are projections on the plane of velocity vectors at cell centres. The colour coding represents the magnitude of the velocity.

Two distinct areas of recirculation can be observed in the centre of the model. Furthermore, the velocity magnitude at each of these discontinuities increases as the coupling interface nears the manifold volume. Examining the centre volume of the manifold, the flow field inside Figs.C-3 and C-5 are similar. However, the results show in Fig. C-7 corresponding to the model without inlet and outlet pipes is markedly different. It is concluded that the short pipe model (Fig. C-5) is the ideal model with which to calculate the flow inside the manifold. The long pipe model (Fig. C3) produces the same results, but the computational effort is greater.

From these examples, it can be seen that the placement of the interface influences the predictions of a coupled 1D/3D calculation. Good practice places the coupling interface in a location where the flow is unaffected by geometrical discontinuities.

The nature of the geometry before the coupling is also important. If, for example, there is a sharp bend in the 1D model directly before the coupling interface to the 3D model, inaccurate results will be produced and the security of the rest of the model will be prejudiced.